NASA TN D-176

TN-02
197237
39P

TECHNICAL NOTE

D-176

WORKING CHARTS FOR RAPID PREDICTION OF FORCE AND PRESSURE COEFFICIENTS ON ARBITRARY BODIES OF REVOLUTION BY USE OF NEWTONIAN CONCEPTS

By Robert W. Rainey

Langley Research Center
Langley Field, Va.

NATIONAL AERONAUTICS AND SPACE ADMINISTRATION

WASHINGTON

December 1959

(NASA-TN-D-176) WORKING CHARTS FOR RAPID PREDICTION OF FORCE AND PRESSURE COEFFICIENTS ON ARBITRARY BODIES OF REVOLUTION BY USE OF NEWTONIAN CONCEPTS (NASA) 39 p

N89-70577

Unclas
00/02 0197237

1Q

NATIONAL AERONAUTICS AND SPACE ADMINISTRATION

TECHNICAL NOTE D-176

WORKING CHARTS FOR RAPID PREDICTION OF FORCE AND PRESSURE COEFFICIENTS ON ARBITRARY BODIES OF REVOLUTION BY USE OF NEWTONIAN CONCEPTS

By Robert W. Rainey

SUMMARY

A simplified method, with working charts, is presented so that the loading, or pressure, distributions and aerodynamic characteristics of arbitrary bodies of revolution may be readily obtained by use of Newtonian concepts. The equations are in such a form as to facilitate an investigation of effects of Mach number variation and changes in specific-heat ratio upon the aerodynamic characteristics.

INTRODUCTION

The use of Newtonian and modified Newtonian theories has proven to be of value in the computation of the pressure, or load, distributions and aerodynamic characteristics of bodies of revolution at supersonic and hypersonic speeds, particularly for cases associated with the detachment of shock waves (for instances, refs. 1 to 3). In order to simplify and expedite such computations for arbitrary bodies of revolution, a method of application of Newtonian concepts (similar to that of ref. 4) with working charts is presented. By use of these curves, the aerodynamic characteristics of an arbitrary body of revolution may be obtained without the computation or radial integration of the pressure distributions. If the pressure, or load, distribution is desired, however, the necessary curves are included for their attainment.

SYMBOLS

A	reference area, πR^2
C_A	axial-force coefficient, $\frac{F_A}{q_\infty A}$

C_m pitching-moment coefficient, $\frac{M_Y}{q_\infty A l}$

$C_{m_\alpha} = \frac{dC_m}{d\alpha}$

C_N normal-force coefficient, $\frac{F_N}{q_\infty A}$

$C_{N_\alpha} = \frac{dC_N}{d\alpha}$

C_p pressure coefficient, $\frac{(p - p_\infty)}{q_\infty}$

F_A axial force of body

F_{A_x} axial force per unit length of element, $\frac{dF_A}{dx}$

F_N normal force of body

F_{N_x} normal force per unit length of element, $\frac{F_N}{dx}$

K $\frac{C_p}{\cos^2\eta}$ (and is usually equal to the stagnation-pressure coefficient)

l body length

l_x distance from moment reference to transverse element, positive when element is forward of moment reference

M_∞ free-stream Mach number

M_Y pitching moment of body due to normal force only

M_{Y_x} pitching moment per unit length of element, $\frac{dM_Y}{dx}$

$\bar{n}$ unit vector normal to surface, positive inward

n_X projection of unit vector on the X-axis

n_Y projection of unit vector on the Y-axis

L 5 1 6

n_Z	projection of unit vector on the Z-axis
p	local static pressure
p_∞	free-stream static pressure
q_∞	free-stream dynamic pressure, $\frac{\gamma}{2} p_\infty M_\infty^2$
R	reference radius
r	radius of an element in the transverse plane
U_∞	free-stream velocity
u	projection of U_∞ on X-axis
v	projection of U_∞ on Y-axis
w	projection of U_∞ on Z-axis
X,Y,Z	body axes
α	angle of attack (located in X-Z plane, fig. 1), $\sin^{-1} \frac{w}{U_\infty \cos \beta}$
β	angle of sideslip, $\sin^{-1} \frac{v}{U_\infty}$
γ	ratio of specific heats
η	angle between free stream and unit vector normal to surface element (see fig. 1)
θ	surface slope
ϕ	roll angle of surface element, referenced to Z-axis, positive counterclockwise looking upstream
ϕ_1	limiting value of roll angle at which the surface element becomes parallel to the free-stream direction

PRESENTATION OF METHOD

In order to compute the aerodynamic characteristics of an arbitrary body without calculating or integrating the pressure distributions, the

equations for the radial pressure distribution of a transverse element are first stated in closed form and substituted (with the appropriate direction-cosine relation) in the general equations for the elemental normal and axial forces, F_{N_X} and F_{A_X}, respectively. Integration of the longitudinal distribution of the elemental normal and axial forces completes the calculation.

Equations Used

Newtonian concepts specify that when the moving stream strikes the body surface the change in the normal component of momentum of the flow is converted into an increment in pressure. From Newtonian concepts, the pressure coefficient of a surface element is

L 5 1 6

$$C_p = K \cos^2\eta \tag{1}$$

where K is dependent upon the type of the body under consideration and the fluid characteristics. (This choice of K is discussed in a subsequent section of this paper.) The derivations of η and the direction cosines were accomplished by the substitution of an element of a tangent cone for the local transverse element dx (fig. 2). The direction cosines for the inner normal vector are

$$\cos A = \frac{n_X}{\bar{n}} = - \sin\theta \tag{2}$$

$$\cos B = \frac{n_Y}{\bar{n}} = - \sin\phi \cos\theta \tag{3}$$

$$\cos C = \frac{n_Z}{\bar{n}} = - \cos\phi \cos\theta \tag{4}$$

and the direction cosines for the velocity vector for a body at α and β are

$$\cos D = \frac{u}{U_\infty} = - \cos\alpha \cos\beta$$

$$\cos E = \frac{v}{U_\infty} = \sin\beta$$

$$\cos F = \frac{w}{U_\infty} = \sin\alpha \cos\beta$$

The quantity $\cos \eta$ is the scalar product of the inner normal vector and the free-stream velocity vector; therefore,

$$\cos \eta = \sin \theta \cos \alpha \cos \beta - \cos \theta \sin \phi \sin \beta$$

$$- \cos \theta \cos \phi \sin \alpha \cos \beta \tag{5}$$

This relation for η is useful for the computation of pressure or load distributions for bodies of revolution at combinations of α and β. Other applications are also possible. For instance, the pressure distribution on the hemicylindrical leading edge of a swept wing at angles of attack may be computed by the substitution of $\theta = 0^\circ$ (for the hemicylinder) and ϵ for β where ϵ is the semiapex angle of the wing and is equal to $\tan^{-1} (\tan \beta / \cos \alpha)$.

L
5
1
6

For the method of rapid prediction to be presented herein, only the arbitrary body of revolution at angles of attack is considered. Therefore, $\beta = 0^\circ$ and

$$\cos \eta = \sin \theta \cos \alpha - \cos \theta \cos \phi \sin \alpha \tag{5a}$$

The value of ϕ at which the unit vector becomes perpendicular to the free stream is the value at which the surface element becomes parallel to the free-stream direction, and ϕ thus specifies the edge of the "shadowed" region. This value of ϕ may be found by substituting $\eta = 90^\circ$ into equation (5a) for which

$$\phi_1 = \cos^{-1} \frac{\tan \theta}{\tan \alpha} \tag{6}$$

For a given body transverse element, the surface is shadowed from the oncoming flow when $\phi < \phi_1$.

With the assumption that $C_p = 0$ in the shadowed region, the elemental normal force of a transverse element dx of an arbitrary body is

$$dN = q_\infty C_p \cos C \, dA$$

$$= q_\infty C_p \cos C \frac{r d\phi}{\cos \theta} dx$$

Therefore,

$$F_{N_x} = \frac{2q_\infty}{\cos \theta} \int_{\phi_1}^{\pi} C_p \cos C \, r \, d\phi$$

Likewise

$$F_{A_x} = \frac{2q_\infty}{\cos\theta} \int_{\phi_1}^{\pi} C_p \cos A \; r \, d\phi \tag{8}$$

$$M_{Y_x} = \frac{2q_\infty}{\cos\theta} \int_{\phi_1}^{\pi} C_p \cos C \; l_x r \, d\phi \tag{9}$$

or substituting from equation (1) and the appropriate direction cosine the following expressions result:

$$\frac{F_{N_x}}{q_\infty} \frac{1}{rK} = 2 \int_{\phi_1}^{\pi} \frac{\cos^2\eta \cos C}{\cos\theta} \, d\phi \tag{10}$$

$$\frac{F_{A_x}}{q_\infty} \frac{1}{rK} = 2 \int_{\phi_1}^{\pi} \frac{\cos^2\eta \cos A}{\cos\theta} \, d\phi \tag{11}$$

$$\frac{M_{Y_x}}{q_\infty} \frac{1}{rK} = 2l_x \int_{\phi_1}^{\pi} \frac{\cos^2\eta \cos C}{\cos\theta} \, d\phi \tag{12}$$

Substitution of the relations for $\cos A$, $\cos C$, and $\cos \eta$ from equations (2), (4), and (5a) and integration (for the case where $\phi > \phi_1$) yield:

$$\begin{aligned} 2 \int_{\phi_1}^{\pi} \frac{\cos^2\eta \cos C}{\cos\theta} \, d\phi = {} & -2 \cos^2\theta \sin^2\alpha \left[\frac{1}{3} \sin\phi(\cos^2\phi + 2)\right]_{\phi_1}^{\pi} \\ & + 4 \sin\theta \cos\theta \cos\alpha \sin\alpha \left[\frac{1}{2} \sin\phi \cos\phi + \frac{\phi}{2}\right]_{\phi_1}^{\pi} \\ & - 2 \sin^2\theta \cos^2\alpha \left[\sin\phi\right]_{\phi_1}^{\pi} \end{aligned} \tag{13}$$

L
5
1
6

$$2\int_{\phi_1}^{\pi}\frac{\cos^2\eta\,\cos A}{\cos\theta}\,d\phi = 2\cos\theta\sin\theta\sin^2\alpha\left[\frac{1}{2}\sin\phi\cos\phi+\frac{\phi}{2}\right]_{\phi_1}^{\pi}$$

$$-4\sin^2\theta\sin\alpha\cos\alpha\left[\sin\phi\right]_{\phi_1}^{\pi}$$

$$+2\frac{\sin^3\theta\cos^2\alpha}{\cos\theta}\left[\phi\right]_{\phi_1}^{\pi} \qquad (14)$$

$$2\int_{\phi_1}^{\pi}\frac{\cos^2\eta\,\cos C}{\cos\theta}\,l_x\,d\phi = -2\cos^2\theta\sin^2\alpha l_x\left[\frac{1}{3}\sin\phi(\cos^2\phi+2)\right]_{\phi_1}^{\pi}$$

$$+4\sin\theta\cos\theta\cos\alpha\sin\alpha l_x\left[\frac{1}{2}\sin\phi\cos\phi\right.$$

$$\left.+\frac{\phi}{2}\right]_{\phi_1}^{\pi}-2\sin^2\theta\cos^2\alpha l_x\left[\sin\phi\right]_{\phi_1}^{\pi} \qquad (15)$$

When $\phi_1 = 0$ (no shadowed region),

$$2\int_{\phi_1}^{\pi}\frac{\cos^2\eta\,\cos C}{\cos\theta}\,d\phi = 2\pi\sin\theta\cos\theta\cos\alpha\sin\alpha \qquad (16)$$

$$2\int_{\phi_1}^{\pi}\frac{\cos^2\eta\,\cos A}{\cos\theta}\,d\phi = \pi\sin\theta\cos\theta\left[\sin^2\alpha+2\tan^2\theta\cos^2\alpha\right] \qquad (17)$$

$$2\int_{\phi_1}^{\pi}\frac{\cos^2\eta\,\cos C}{\cos\theta}\,l_x\,d\phi = 2\pi l_x\sin\theta\cos\theta\cos\alpha\sin\alpha \qquad (18)$$

For an arbitrary body of revolution,

$$C_N = \frac{2l}{\pi R^2} \int_0^1 \int_{\phi_1}^{\pi} \frac{C_p \cos C \; r}{\cos \theta} \, d\phi \, d\left(\frac{x}{l}\right)$$

$$= \frac{K}{\pi} \frac{l}{R} \int_0^1 \left[2 \int_{\phi_1}^{\pi} \frac{\cos^2\eta \cos C}{\cos \theta} \, d\phi \right] \frac{r}{R} \, d\left(\frac{x}{l}\right) \tag{19}$$

$$C_A = \frac{2l}{\pi R^2} \int_0^1 \int_{\phi_1}^{\pi} \frac{C_p \cos A \; r}{\cos \theta} \, d\phi \, d\left(\frac{x}{l}\right)$$

$$= \frac{K}{\pi} \frac{l}{R} \int_0^1 \left[2 \int_{\phi_1}^{\pi} \frac{\cos^2\eta \cos A}{\cos \theta} \, d\phi \right] \frac{r}{R} \, d\left(\frac{x}{l}\right) \tag{20}$$

$$C_m = \frac{2l}{\pi R^2} \int_0^1 \int_{\phi_1}^{\pi} \frac{C_p \cos C \; r}{\cos \theta} \frac{l_x}{l} \, d\phi \, d\left(\frac{x}{l}\right)$$

$$= \frac{K}{\pi} \frac{l}{R} \int_0^1 \left[2 \int_{\phi_1}^{\pi} \frac{\cos^2\eta \cos C}{\cos \theta} \, d\phi \right] \frac{l_x}{l} \frac{r}{R} \, d\left(\frac{x}{l}\right) \tag{21}$$

The integrals in the brackets (also see eqs. (6) and (13) to (18)) have been numerically evaluated for various values of $\theta \geq 0^\circ$ and $\alpha \geq 0^\circ$ (and for $l_x/l = 1$ in the case of eq. (21)) and are presented in figures 3 and 4. It should be noted that in figure 3 as $\theta \to 90^\circ$, $2 \int_{\phi_1}^{\pi} \frac{\cos^2\eta \cos A}{\cos \theta} \, d\phi \to \infty$; this results because $\cos \theta \to 0$ in the denominator of the expression $\frac{\cos^2\eta \cos A}{\cos \theta}$ (see eq. (11)). For cases where $\theta = 90^\circ$, the "flat-plate" Newtonian contributions may be computed separately.

Also included are curves of $\cos^2\eta$ plotted against θ for various values of α (fig. 5) throughout the range of roll angles ϕ from 0° to 180°. These were obtained by use of equation (5a) for application in equation (1) for the rapid calculation of pressure, or load, distributions. The boundary of the shadowed region, which determines the minimum

value of ϕ for which figure 5 may be utilized, may be obtained from figure 6, which presents ϕ_1 (from eq. (6)) plotted against θ for various values of α.

An additional item of interest to those concerned with the characteristics of bodies of revolution in the low angle-of-attack range, where no shadowed region exists, is the fact that the values of C_{N_α} and C_{m_α} are essentially constant up to $\alpha \approx 4^\circ$. This may be seen by substituting equations (16) and (18) into equations (19) and (21), respectively, and differentiating, which yields

$$C_{N_\alpha} = 2K \frac{l}{R} \int_0^1 \sin\theta \cos\theta \cos 2\alpha \frac{r}{R} d\left(\frac{x}{l}\right)$$

and

$$C_{m_\alpha} = 2K \frac{l}{R} \int_0^1 \sin\theta \cos\theta \cos 2\alpha \frac{l_x}{l} \frac{r}{R} d\left(\frac{x}{l}\right)$$

For an arbitrary body whose characteristics are computed by this method, C_{N_α} and C_{m_α} would differ by only 1 percent at $\alpha = 4.05^\circ$ and by 6 percent at $\alpha = 9.8^\circ$ from the values of C_{N_α} or C_{m_α} at $\alpha = 0^\circ$.

This result may also be illustrated for a specific case; for instance, for the cone where $x/l = r/R$

$$C_{N_\alpha} = K \cos^2\theta \cos 2\alpha$$

and, with the moment reference at the cone apex,

$$C_{m_\alpha} = \frac{2}{3} K \cos^2\theta \cos 2\alpha$$

and the same relative values of C_{N_α} and C_{m_α} apply as cited for the general case.

Selection of K

The value of K according to Newtonian theory is 2 (when $M_\infty = \infty$, and $\gamma = 1$); however, this value does not account for either Mach

number variation or differences in γ. For blunt bodies it has been suggested that the value of the stagnation-point pressure coefficient be used for K (refs. 5 and 6); that is,

$$K = C_{p_{stag}} = \frac{\gamma + 3}{\gamma + 1}\left[1 - \frac{2}{\gamma + 3}\frac{1}{M_\infty{}^2}\right] \tag{22}$$

For pointed bodies with attached shocks, a slightly higher value of K appears in order, and the Newtonian value of 2 is suggested. As an example, for cones with $\theta \geq 15^\circ$, the Newtonian theory (K = 2) will predict C_{N_α} within 4 percent of the exact values given in reference 7 at Mach numbers greater than 3. The effects of γ variation may be accounted for by use of the hypersonic tangent-cone approximation (refs. 6 and 8).

L 5 1 6

Typical Application of Method

A typical example is presented to illustrate the method of application:

Find the coefficients C_N, C_A, and C_m at angles of attack up to 6° of a second-power body of revolution of fineness ratio 1 with the center of gravity at 50 percent of the body length at a Mach number of 3.55 in air. For this center-of-gravity location, $l_x/l = 0.50 - x/l$.

For a fineness ratio of 1, the equation of the body is

$$x = \frac{4}{l} r^2$$

and the surface slope, $\frac{dr}{dx} = \frac{1}{4\sqrt{x/l}}$. For this blunt-nosed body, K = 1.78.

The steps in the computation are:

(a) Compute the values of r/R and θ at various longitudinal stations x/l (see fig. 7(a)).

(b) Read the appropriate values of $2\int_{\phi_1}^{\pi} \frac{\cos^2\eta \cos A}{\cos\theta} d\phi$ and $2\int_{\phi_1}^{\pi} \frac{\cos^2\eta \cos C}{\cos\theta} d\phi$ from figures 3 and 4, respectively, for various values of θ (obtained from fig. 7(a)).

(c) For the axial- and normal-force coefficient computations, multiply the above values of the integrals by r/R and plot those products against x/l. For the C_m computation, the product of $2\int_{\phi_1}^{\pi} \frac{\cos^2\eta \cos C}{\cos\theta} d\phi$, r/R, and $(0.50 - x/l)$ must be plotted against x/l. (See figs. 7(b), 7(c), and 7(d).)

(d) Integrate the areas prescribed by the above curves and multiply by $\frac{K}{\pi}\frac{l}{R}$ to obtain the aerodynamic coefficients.

(e) Perform steps (a) to (d) for the other angles of attack.

The aerodynamic characteristics computed by the method described are presented in figure 8.

CONCLUDING REMARKS

A simplified method, with working charts, is presented so that the loading, or pressure, distributions and aerodynamic characteristics of arbitrary bodies of revolution may be readily obtained by use of Newtonian concepts. The equations are in such a form as to facilitate the investigation of effects of Mach number variation and changes in specific-heat ratio upon the aerodynamic characteristics.

Langley Research Center,
National Aeronautics and Space Administration,
Langley Field, Va., September 1, 1959.

REFERENCES

1. Oliver, Robert E.: An Experimental Investigation of Flow Over Simple Blunt Bodies at a Nominal Mach Number of 5.8. GALCIT Memo. No. 26 (Contract No. DA-04-495-Ord-19), June 1, 1955.

2. Crawford, Davis H., and McCauley, William D.: Investigation of the Laminar Aerodynamic Heat-Transfer Characteristics of a Hemisphere-Cylinder in the Langley 11-Inch Hypersonic Tunnel at a Mach Number of 6.8. NACA Rep. 1323, 1957. (Supersedes NACA TN 3706.)

3. McLellan, Charles H.: Exploratory Wind-Tunnel Investigation of Wings and Bodies at M = 6.9. Jour. Aero. Sci., vol. 18, no. 10, Oct. 1951, pp. 641-648.

4. Grimminger, G., Williams, E. P., and Young, G. B. W.: Lift on Inclined Bodies of Revolution in Hypersonic Flow. Jour. Aero. Sci., vol. 17, no. 11, Nov. 1950, pp. 675-690.

5. Penland, Jim A.: Aerodynamic Characteristics of a Circular Cylinder at Mach Number 6.86 and Angles of Attack up to 90°. NACA TN 3861, 1957. (Supersedes NACA RM L54A14.)

6. Lees, Lester: Hypersonic Flow. Fifth International Aeronautical Conference (Los Angeles, Calif., June 20-23, 1955), Inst. Aero. Sci., Inc., 1955, pp. 241-276.

7. Staff of the Computing Section, Center of Analysis (Under Direction of Zdeněk Kopal): Tables of Supersonic Flow Around Yawing Cones. Tech. Rep. No. 3 (NOrd Contract No. 9169), M.I.T., 1947.

8. Love, Eugene S., Henderson, Arthur, Jr., and Bertram, Mitchel H.: Some Aspects of Air-Helium Simulation and Hypersonic Approximations. NASA TN D-49, 1959.

L 5 1 6

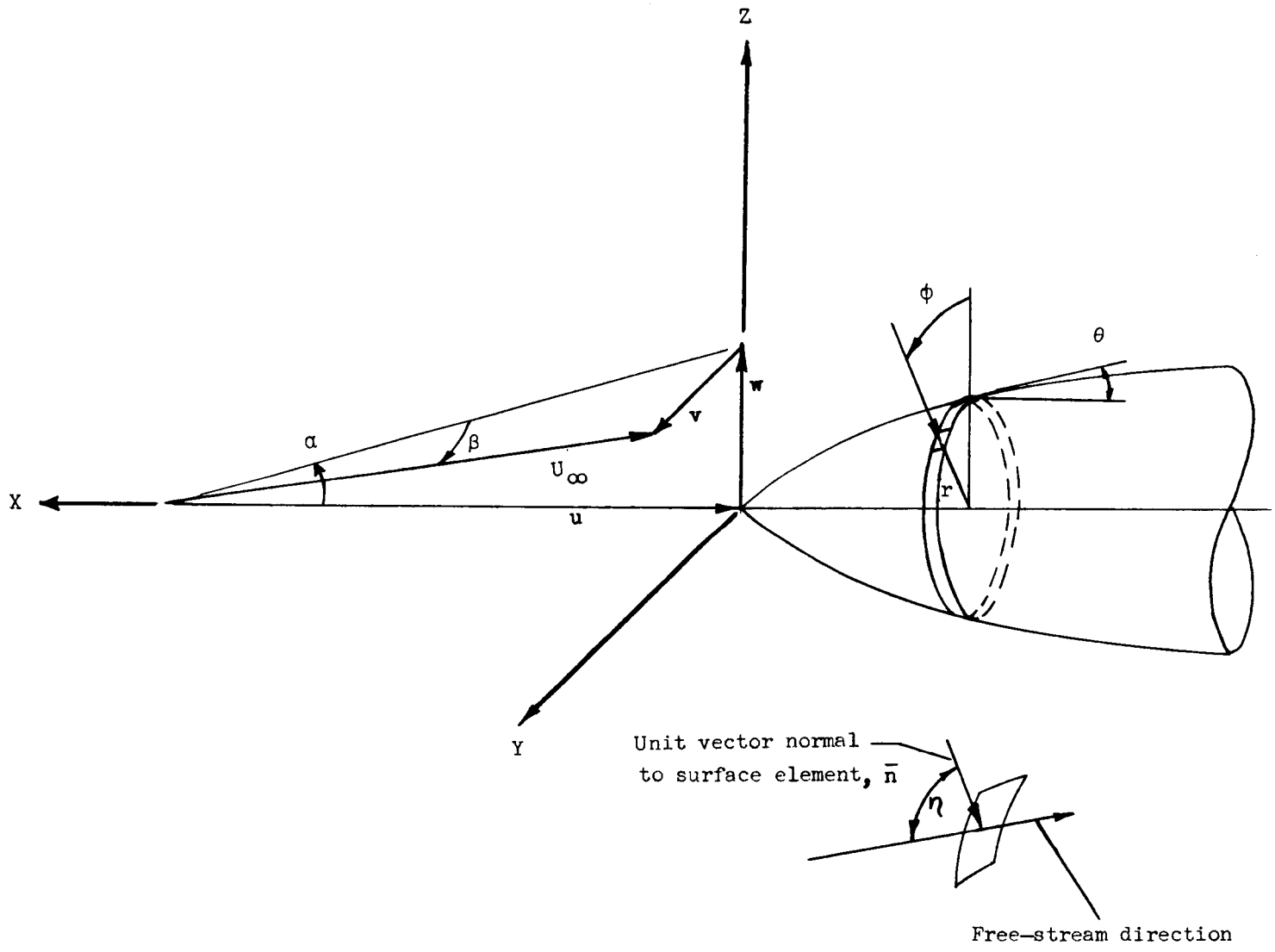

Figure 1.- Definition of axes and symbols.

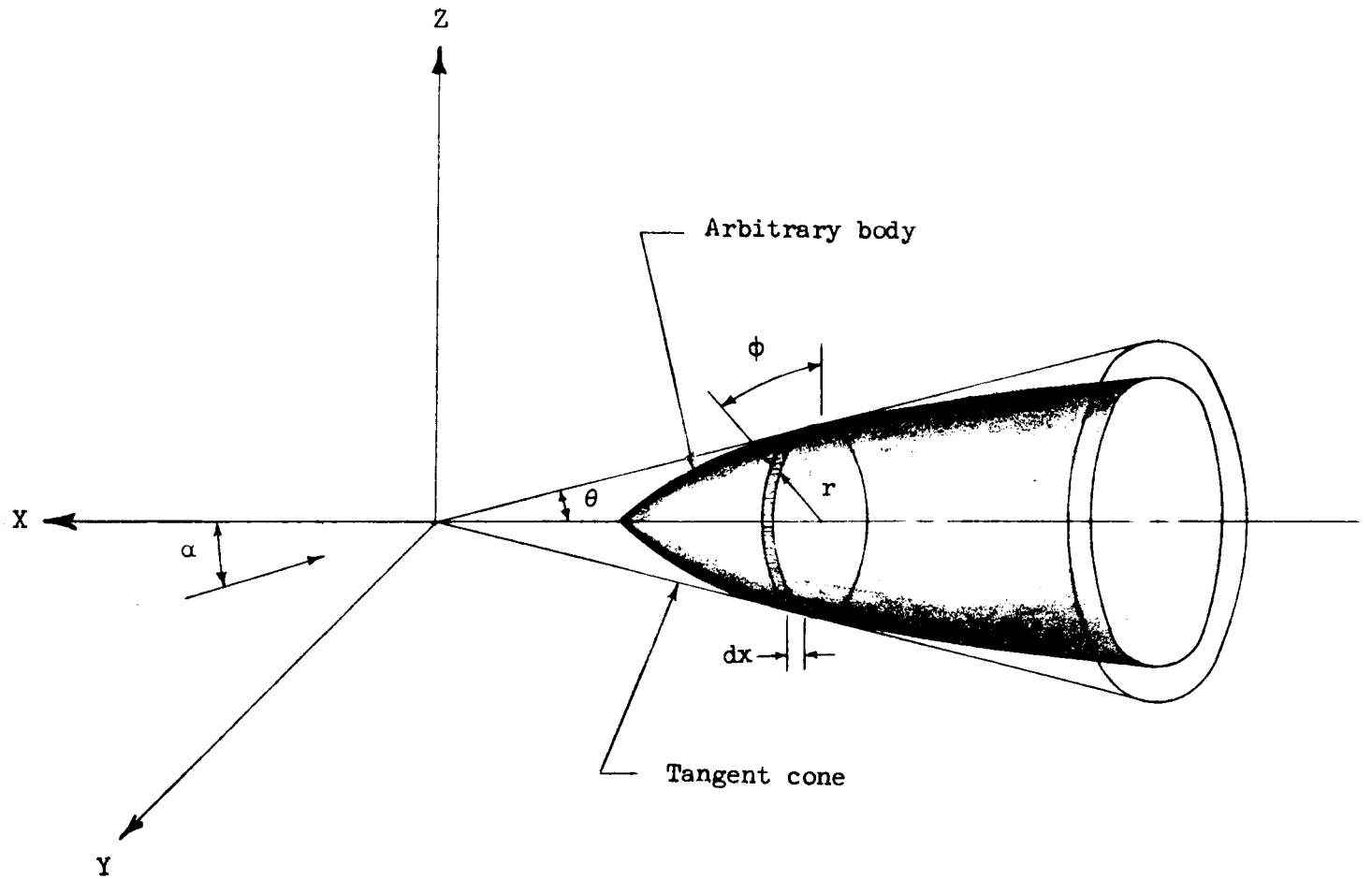

Figure 2.- Tangent cone. Equation of cone: $x^2\tan^2\theta - y^2 - z^2 = 0$.

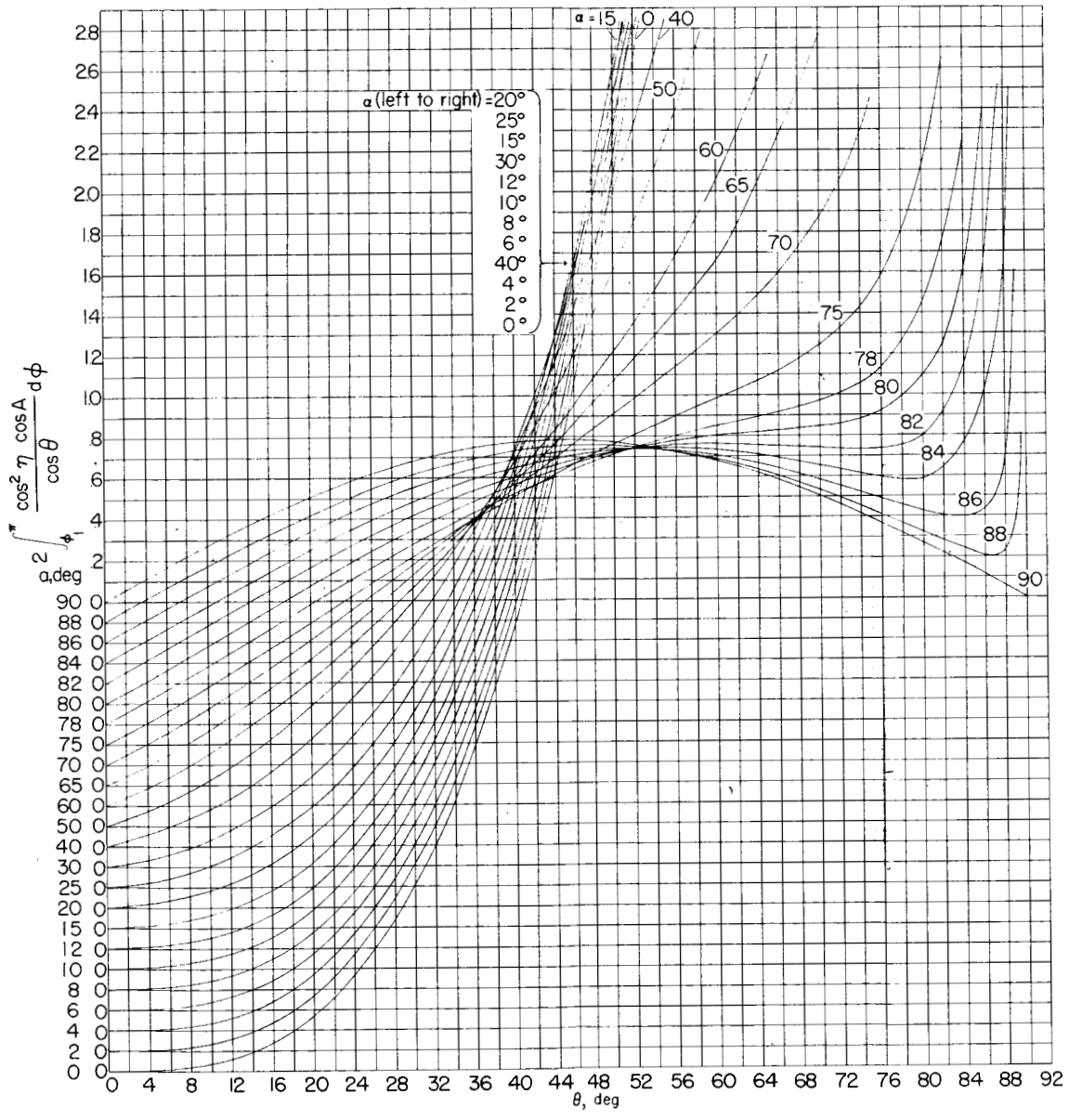

(a) $0^\circ \leqq \theta \leqq 90^\circ$; $0^\circ \leqq \alpha \leqq 90^\circ$.

Figure 3.- Parameter for axial-force computation.

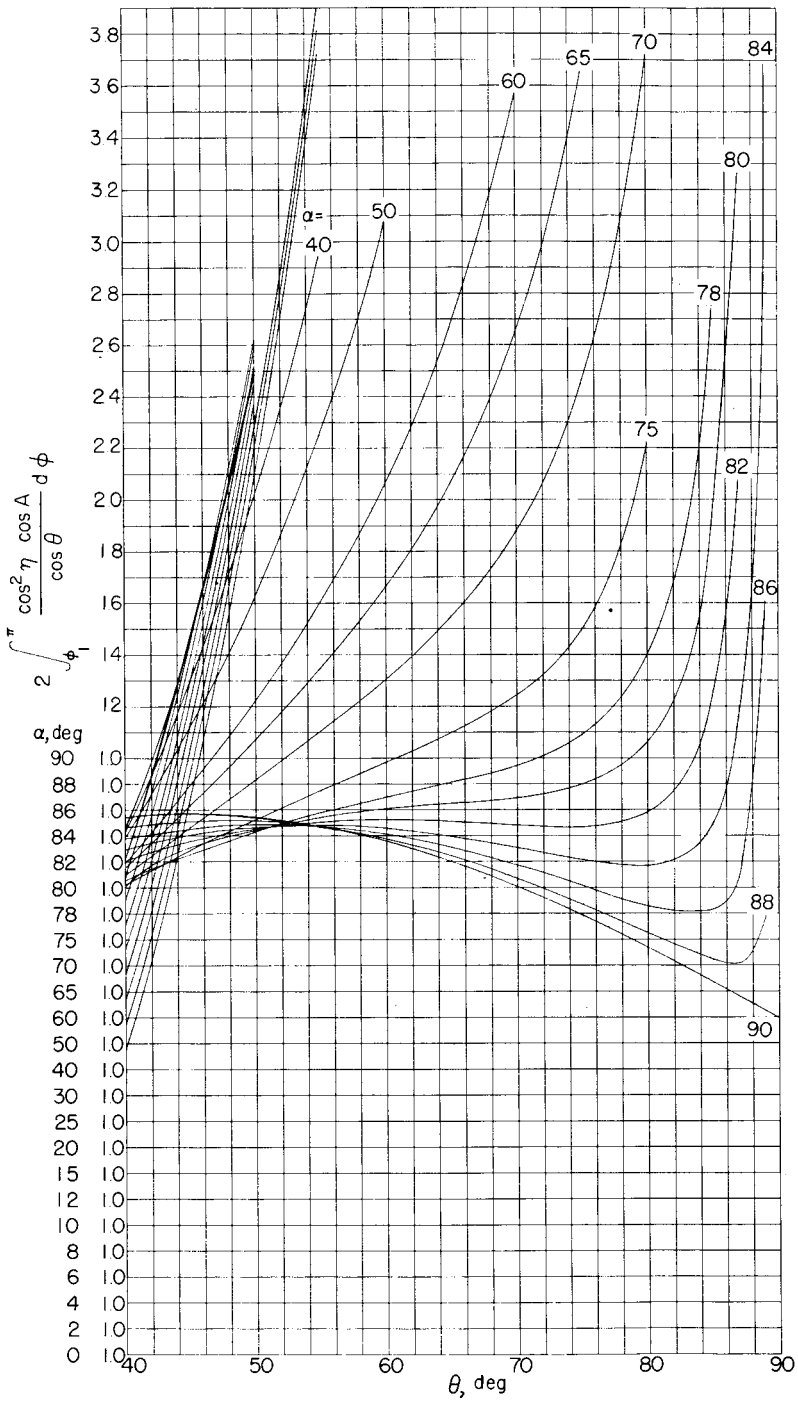

(b) $40^\circ \leqq \theta \leqq 90^\circ$; $0^\circ \leqq \alpha \leqq 90^\circ$.

Figure 3.- Continued.

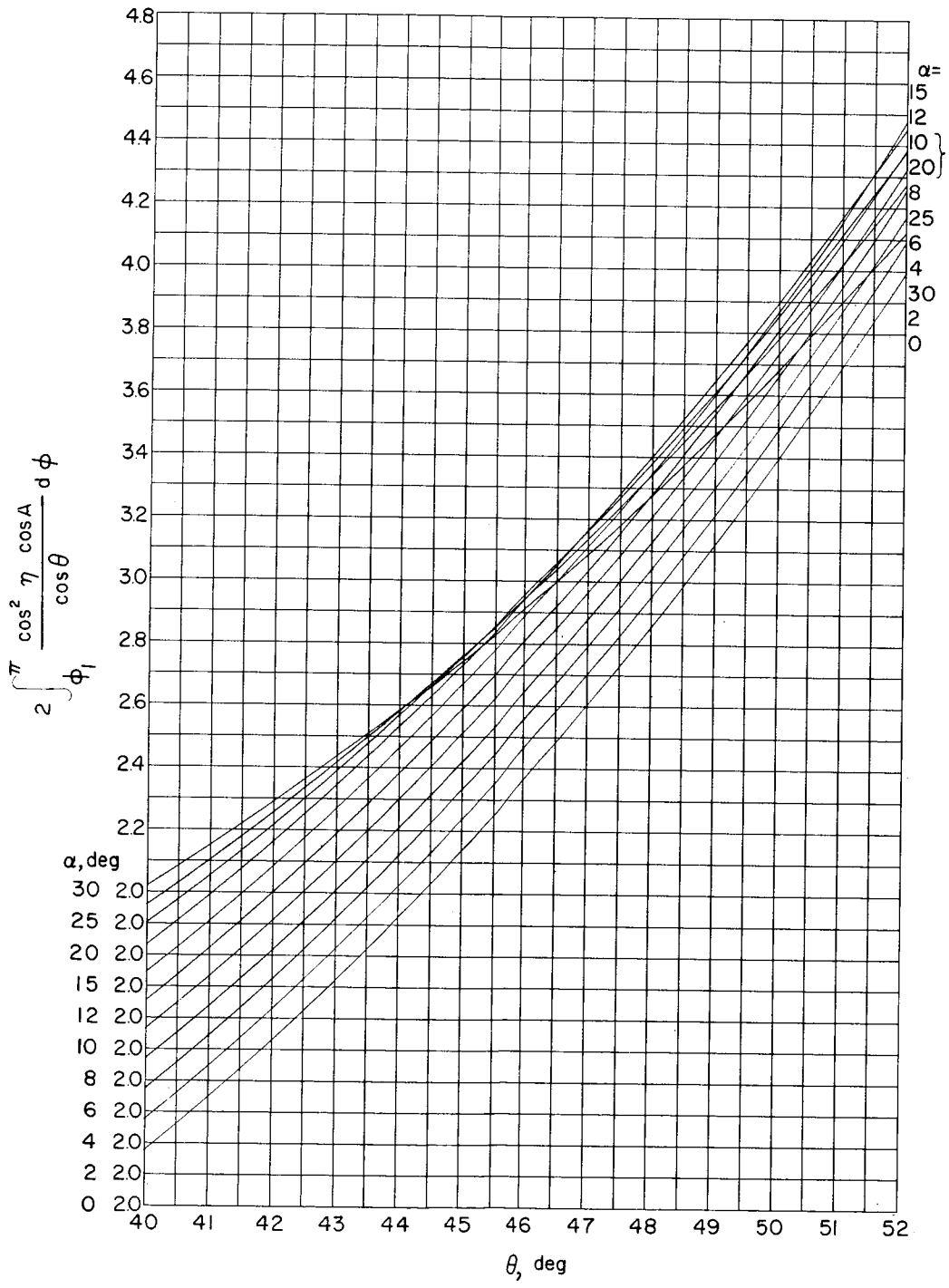

(c) $40^\circ \leq \theta \leq 52^\circ$; $0^\circ \leq \alpha \leq 30^\circ$.

Figure 3.- Continued.

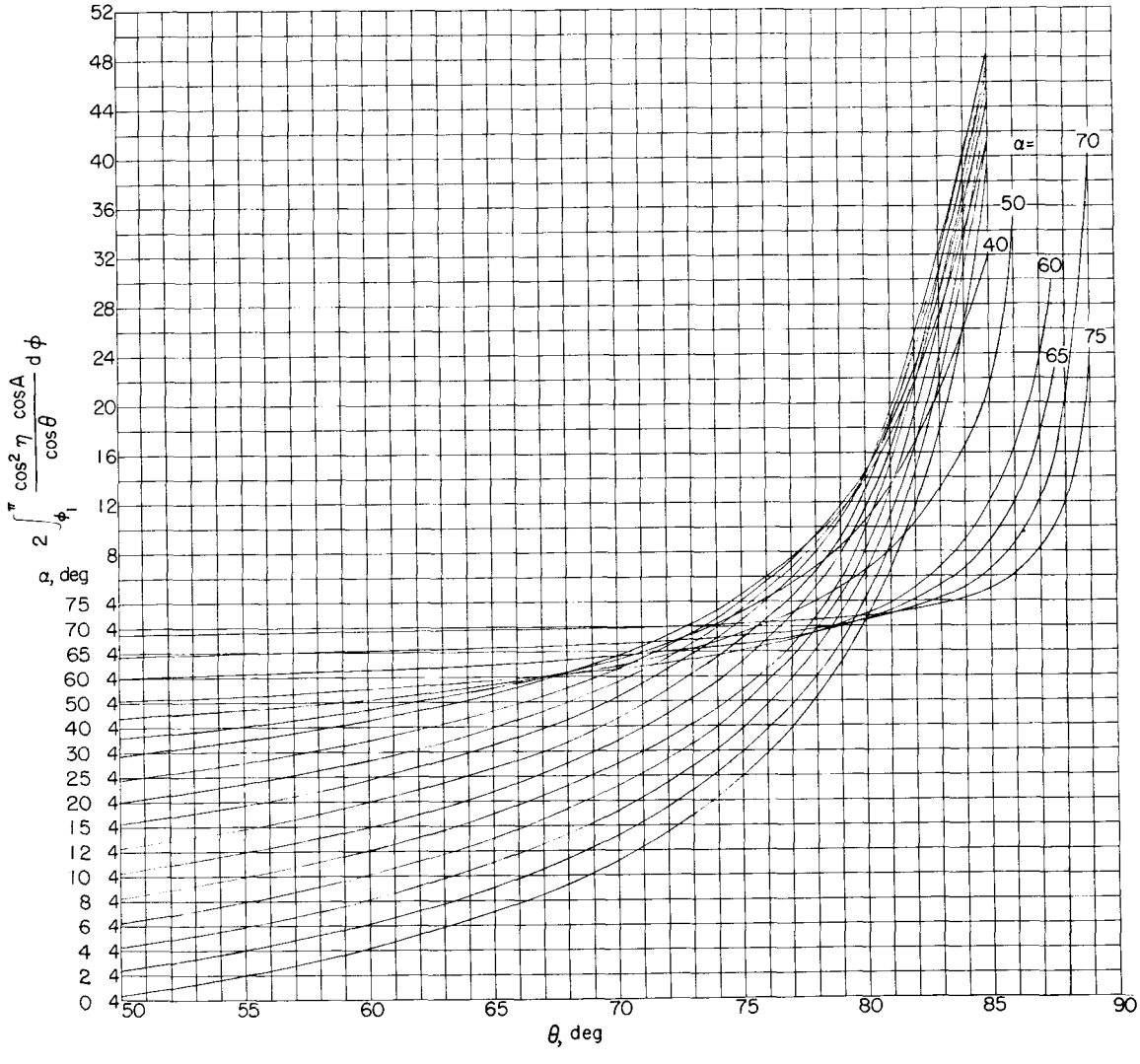

(d) $50^\circ \leqq \theta \leqq 90^\circ$; $0^\circ \leqq \alpha \leqq 75^\circ$.

Figure 3.- Concluded.

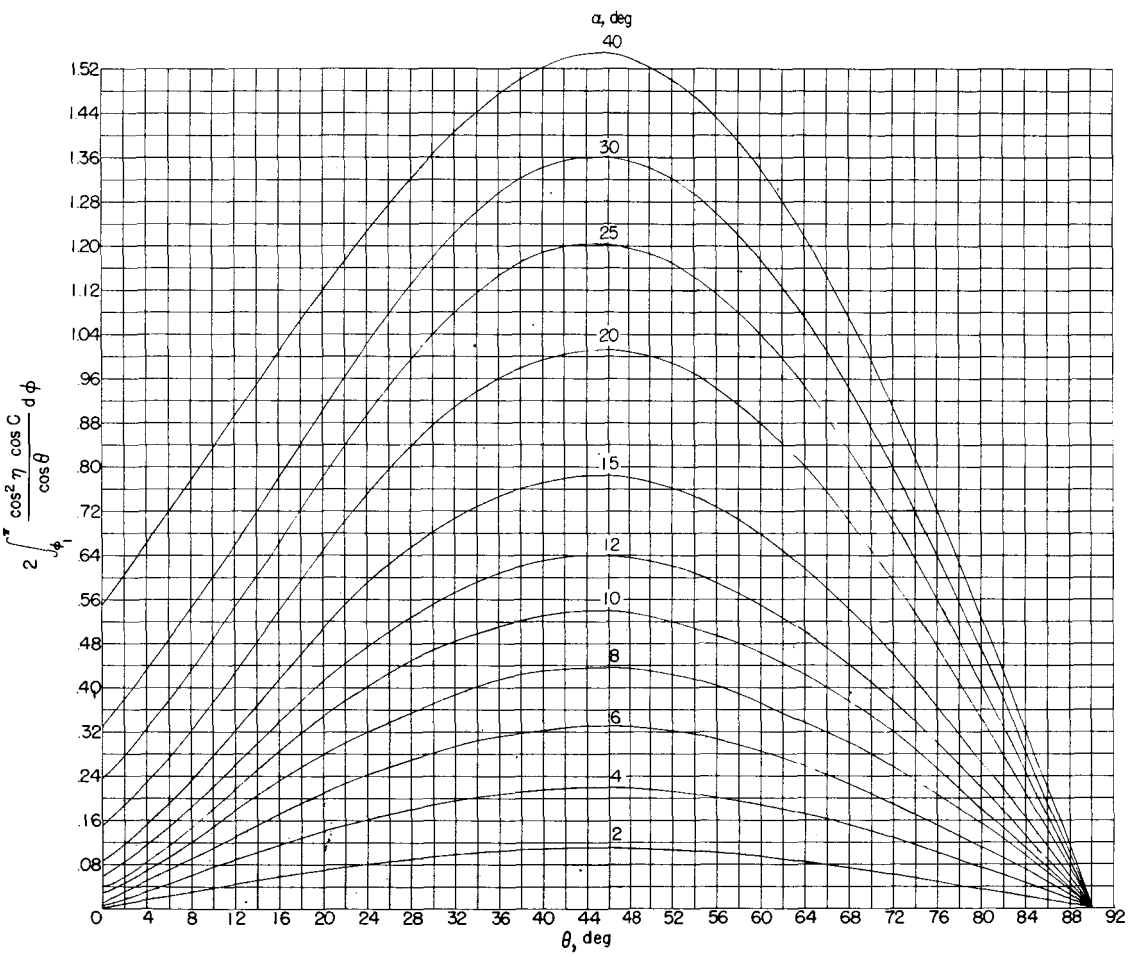

(a) $0^\circ \leq \theta \leq 90^\circ$; $0^\circ \leq \alpha \leq 40^\circ$.

Figure 4.- Parameter of normal-force and pitching-moment computation.

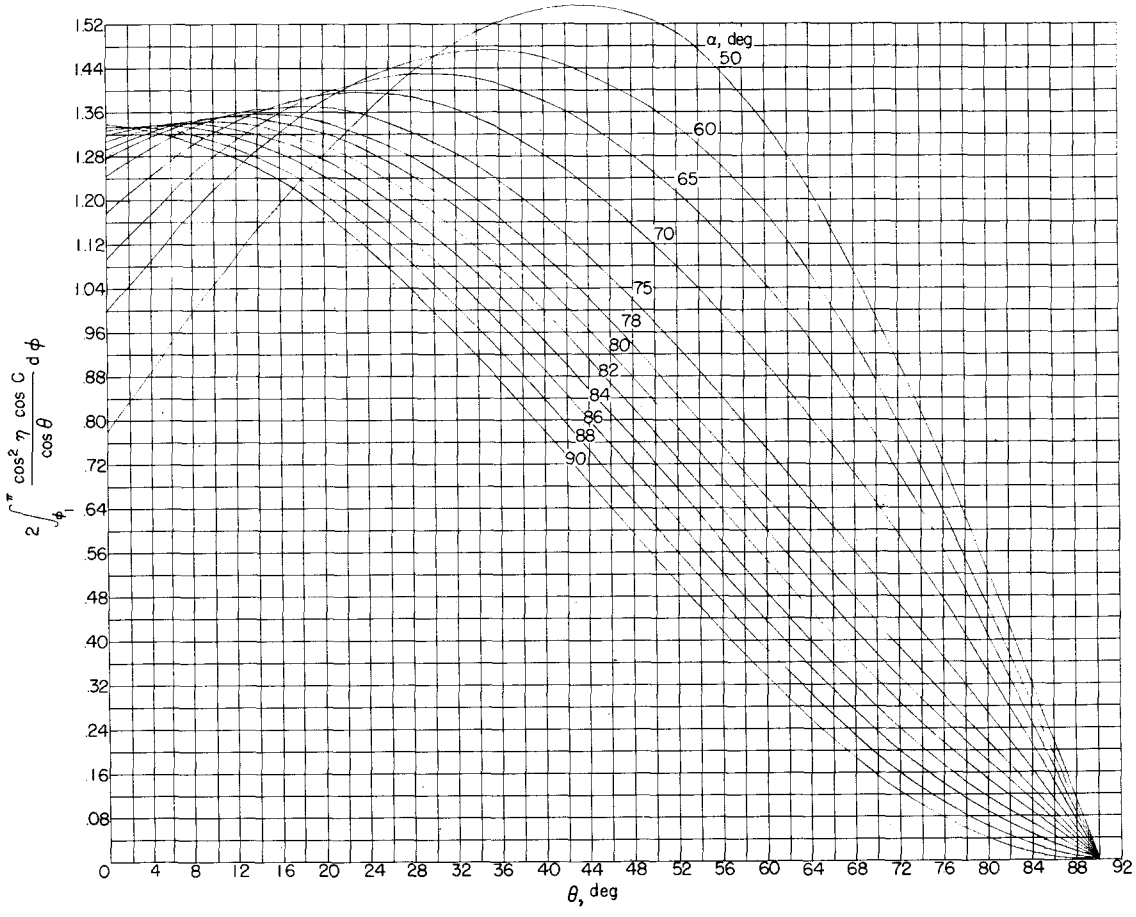

(b) $0° \leqq \theta \leqq 90°$; $50° \leqq \alpha \leqq 90°$.

Figure 4.- Concluded.

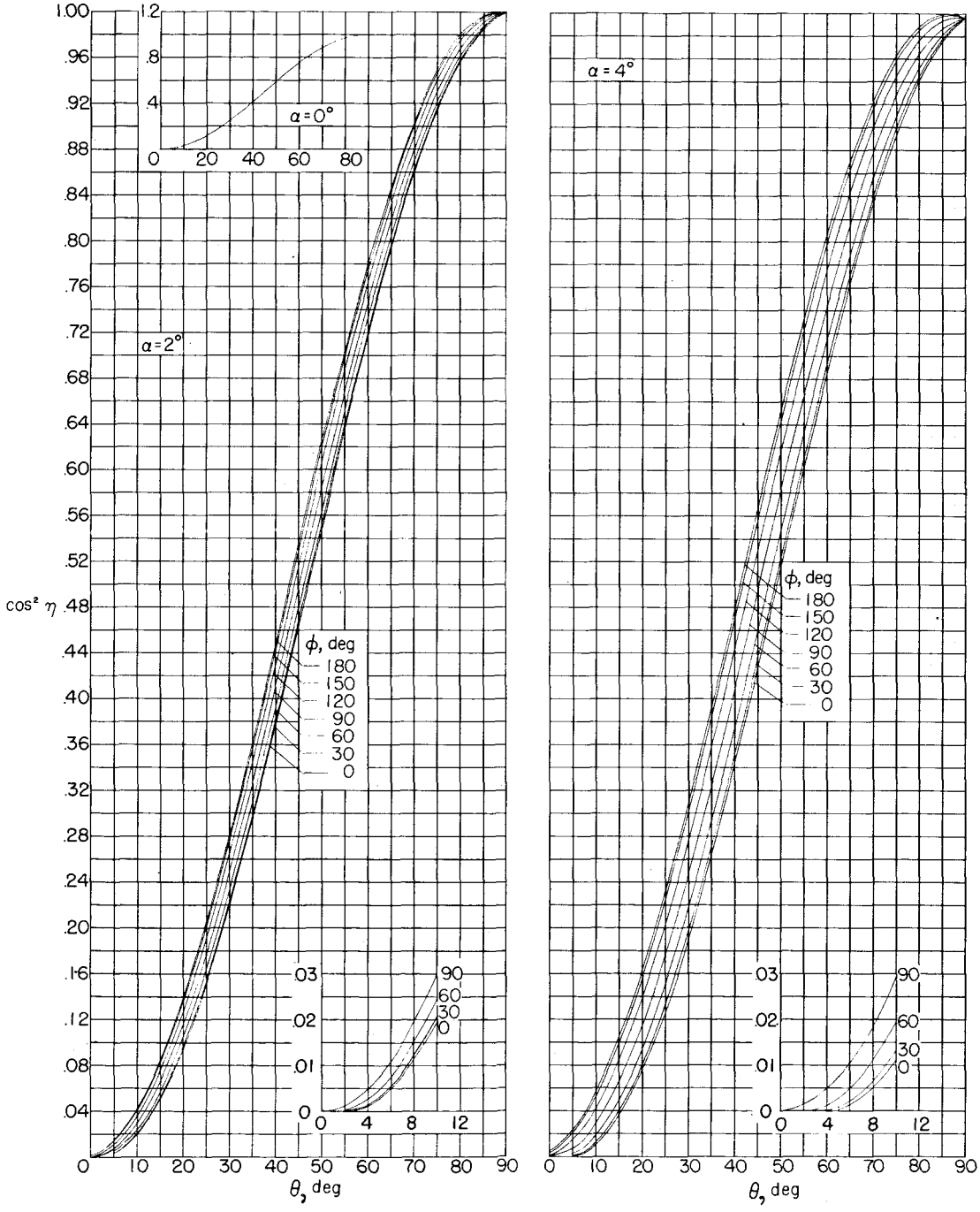

(a) $\alpha = 0^{\circ}$, 2°, and 4°.

Figure 5.- Parameter for pressure-coefficient computations.

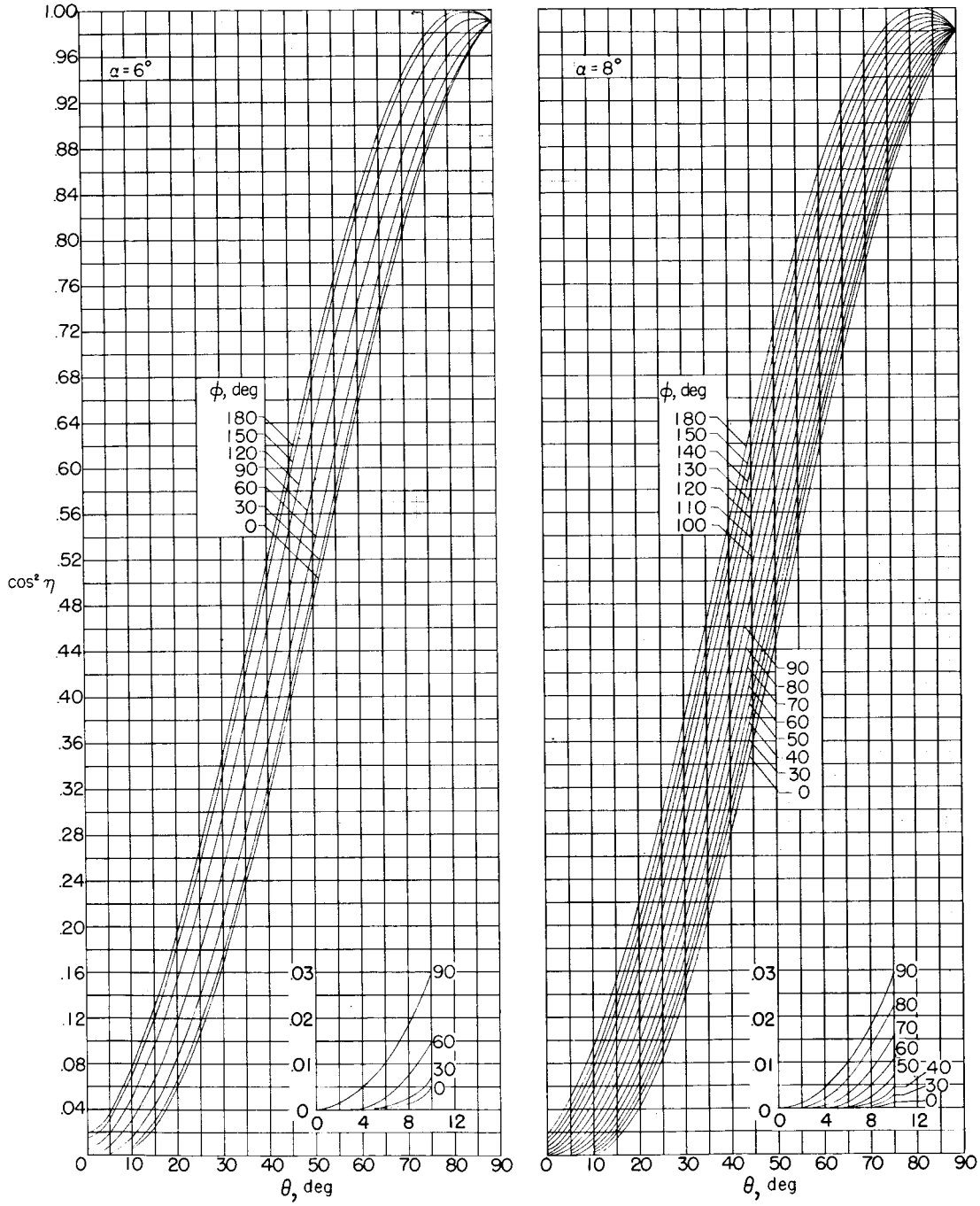

(b) $\alpha = 6^{\circ}$ and 8°.

Figure 5.- Continued.

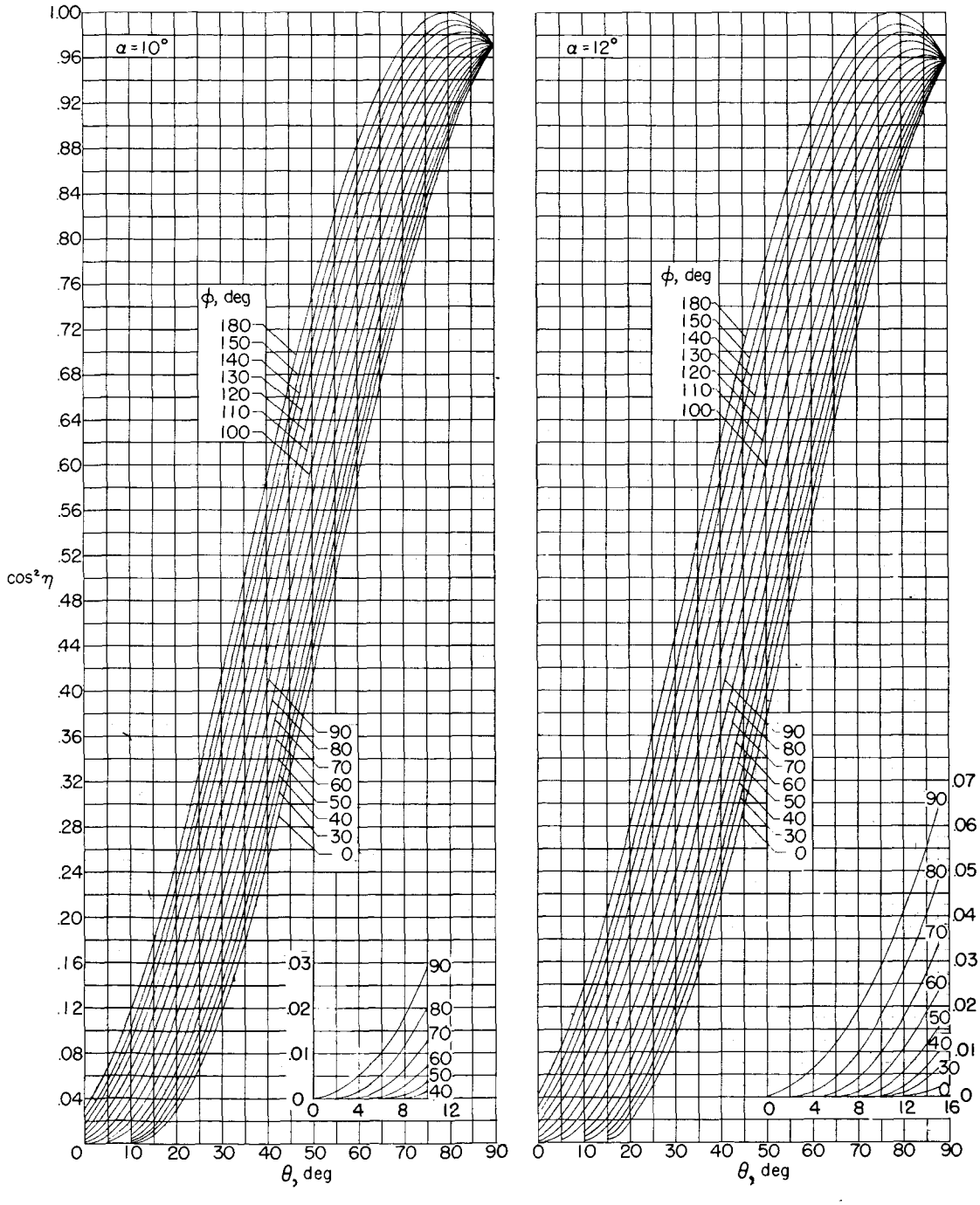

(c) $\alpha = 10^{\circ}$ and 12°.

Figure 5.- Continued.

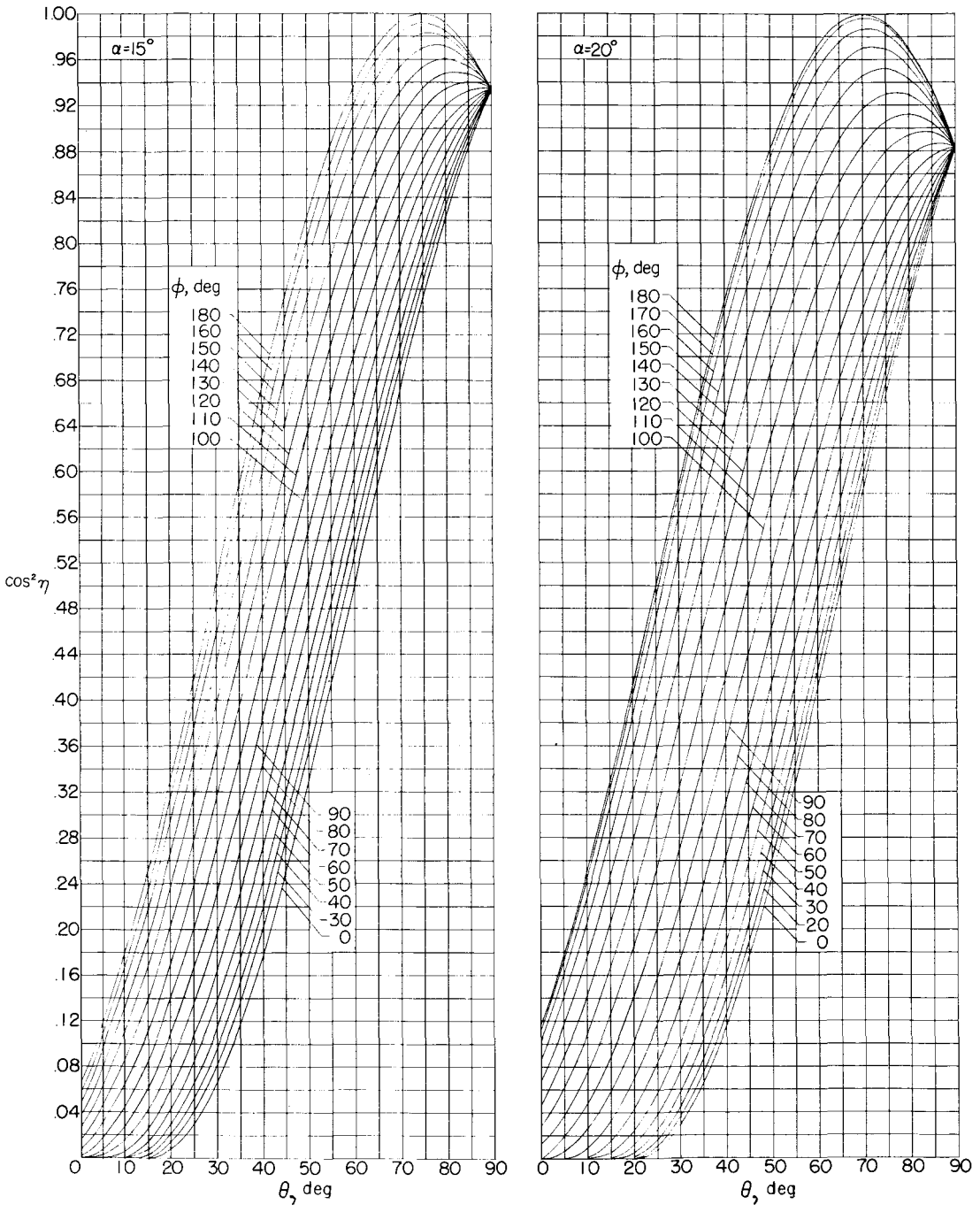

(d) $\alpha = 15^{\circ}$ and 20°.

Figure 5.- Continued.

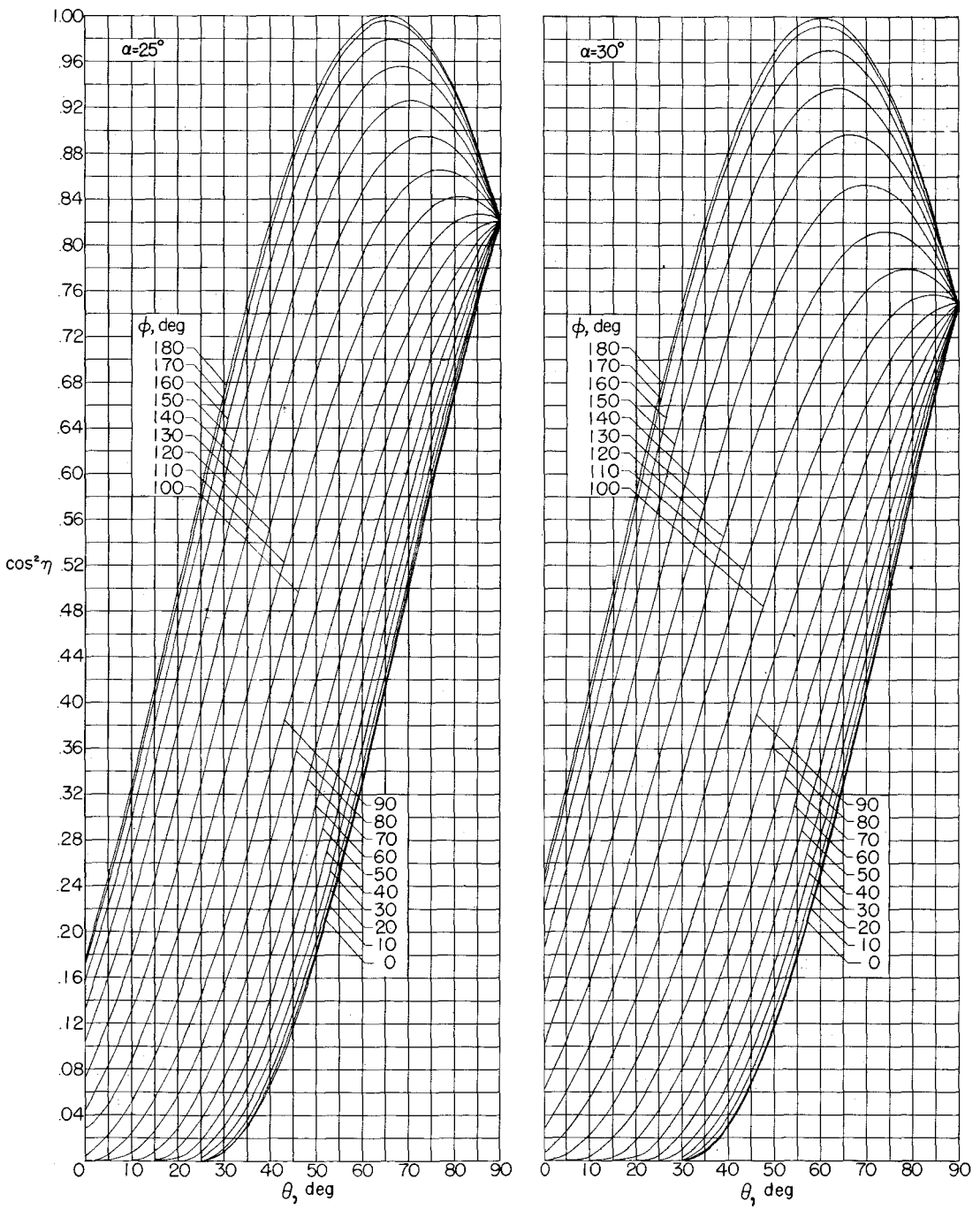

(e) $\alpha = 25^\circ$ and 30°.

Figure 5.- Continued.

L-516

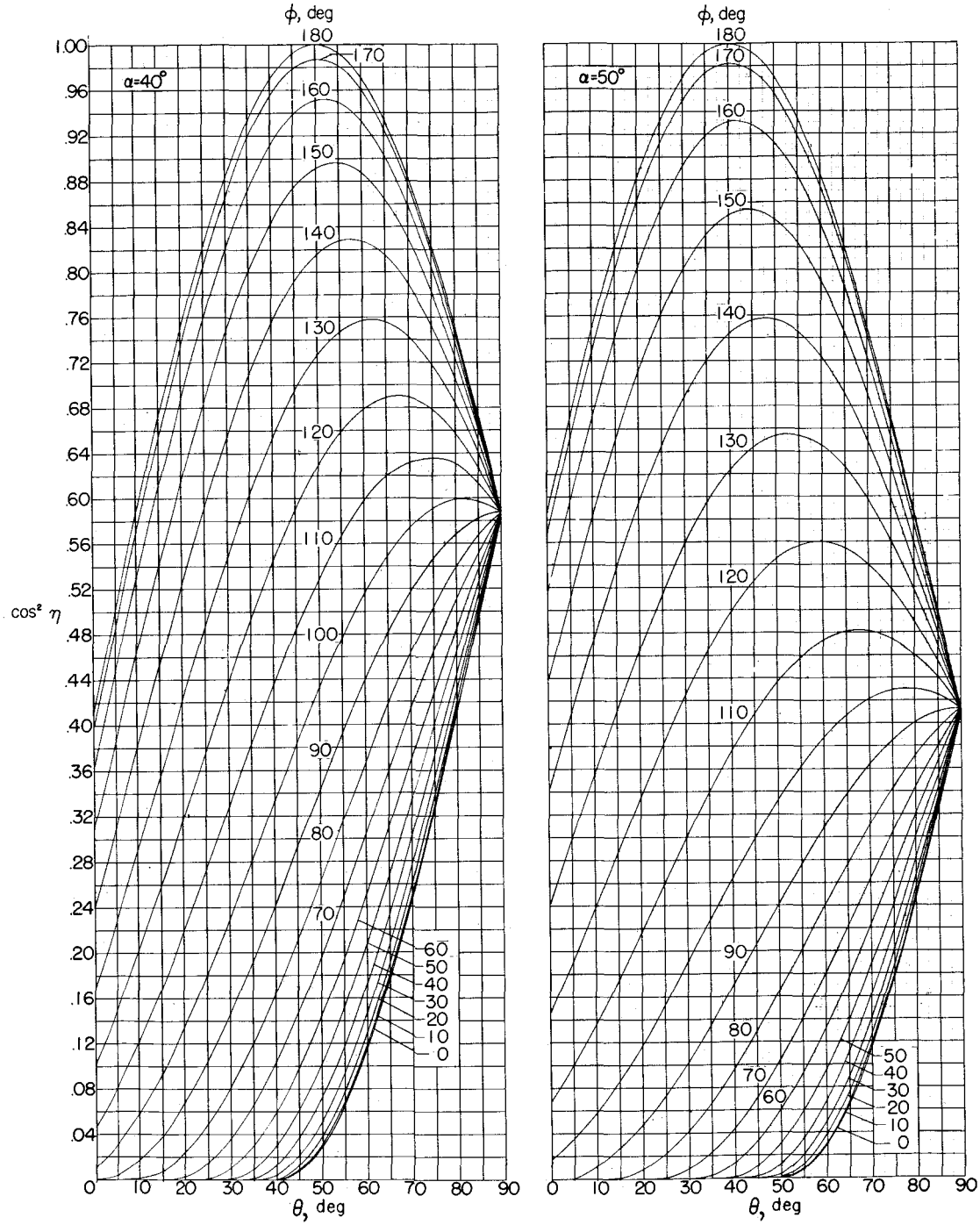

(f) $\alpha = 40^\circ$ and 50°.

Figure 5.- Continued.

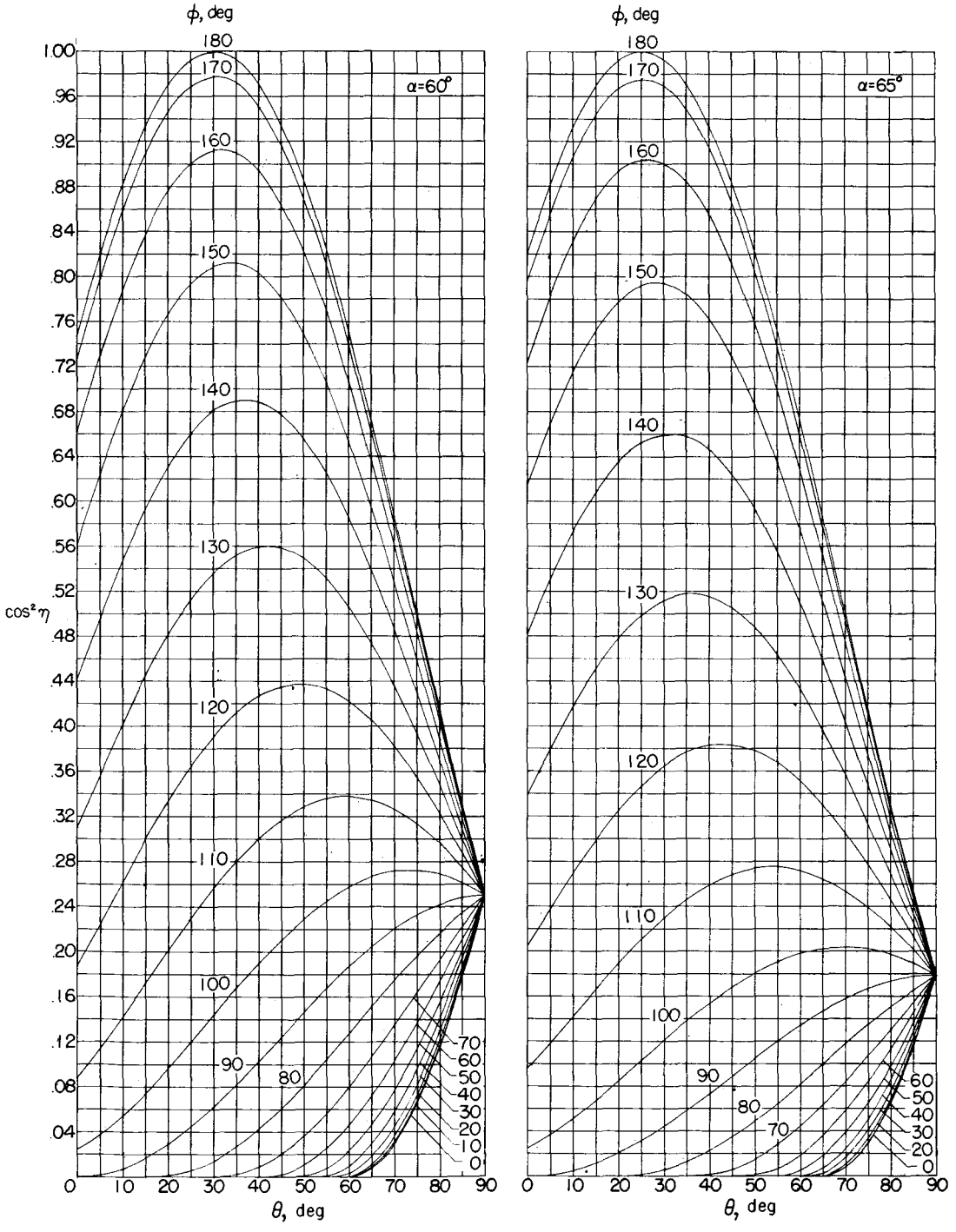

(g) $\alpha = 60^{\circ}$ and 65°.

Figure 5.- Continued.

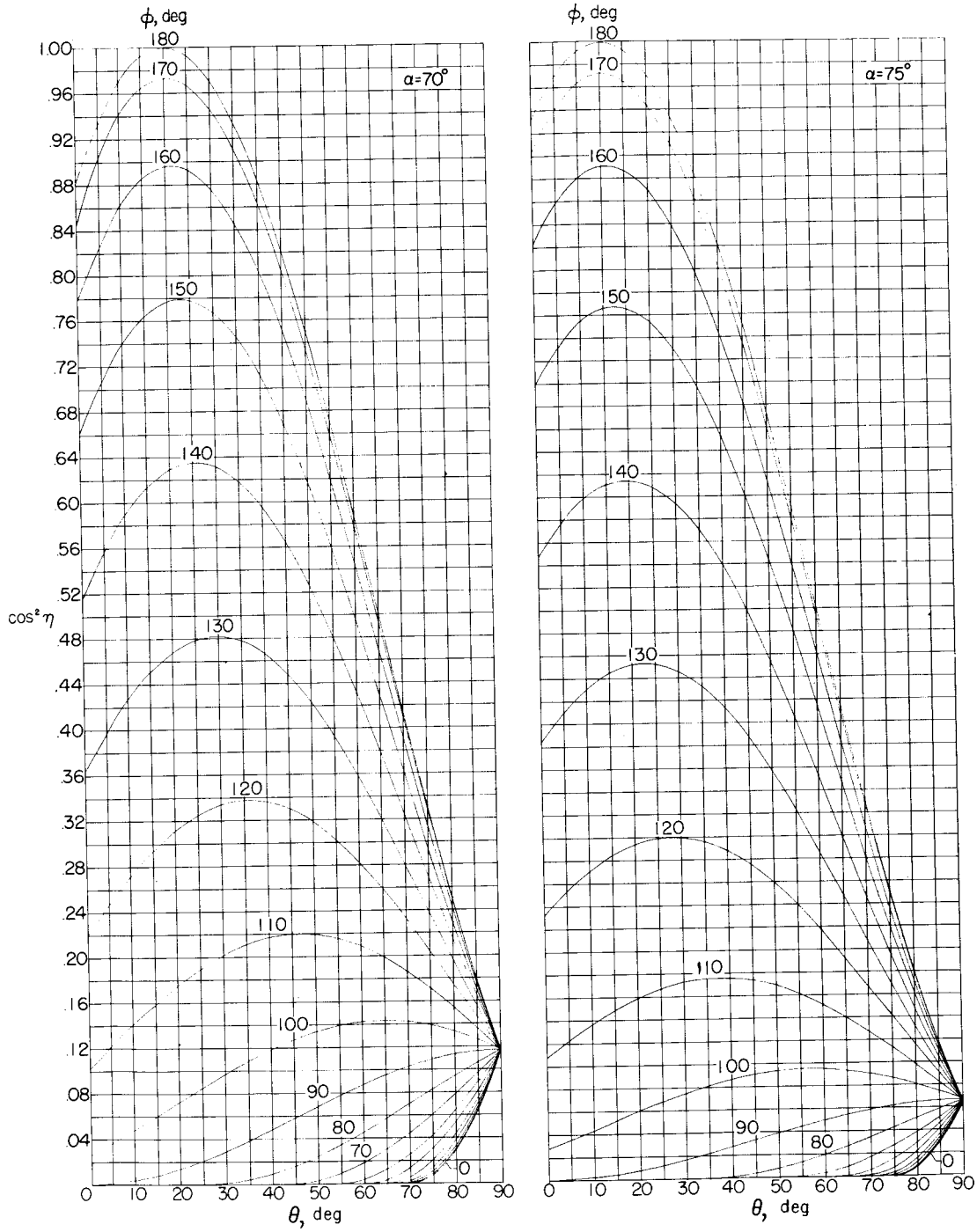

(h) $\alpha = 70^{\circ}$ and 75°.

Figure 5.- Continued.

L-516

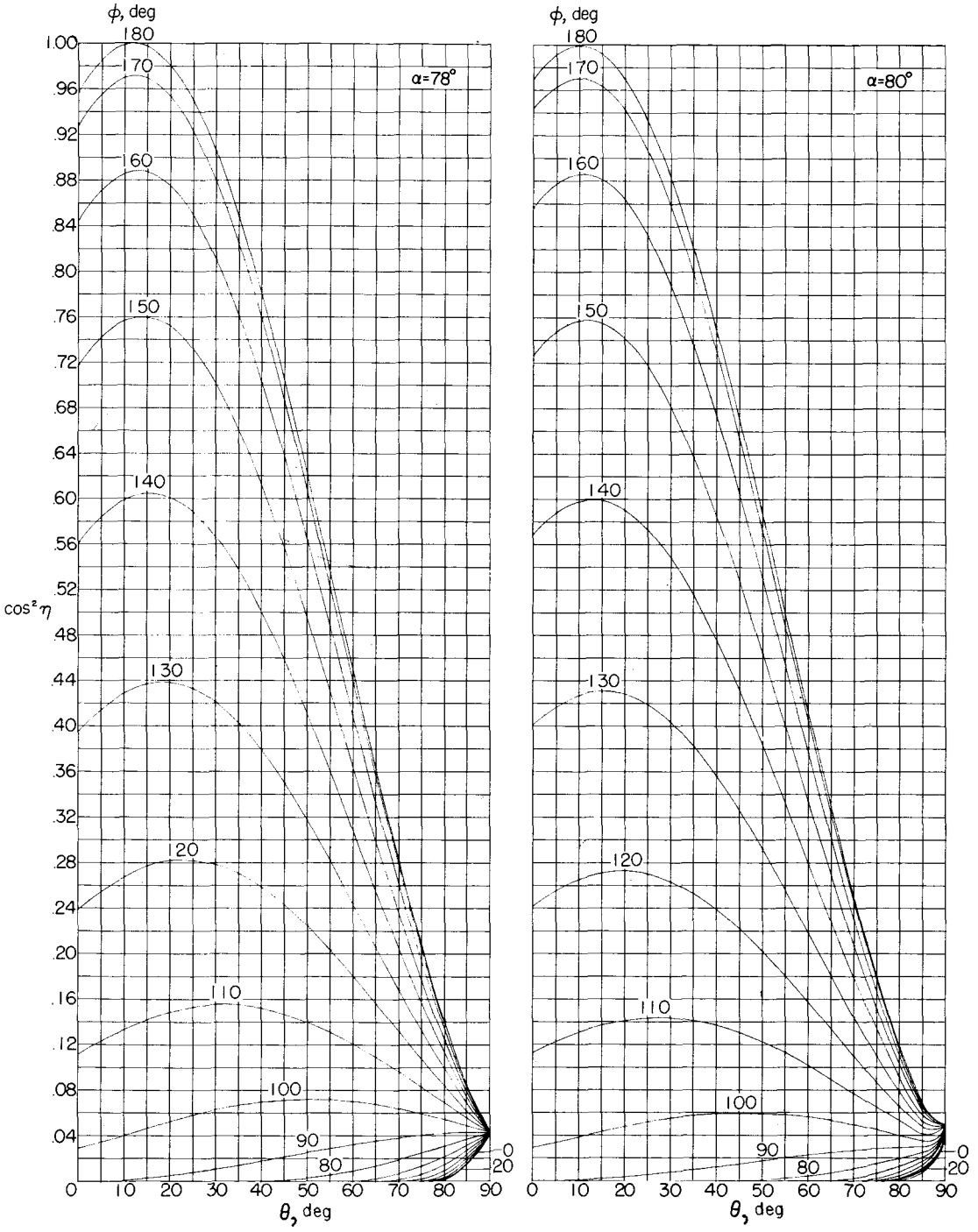

(i) $\alpha = 78^{\circ}$ and 80°.

Figure 5.- Continued.

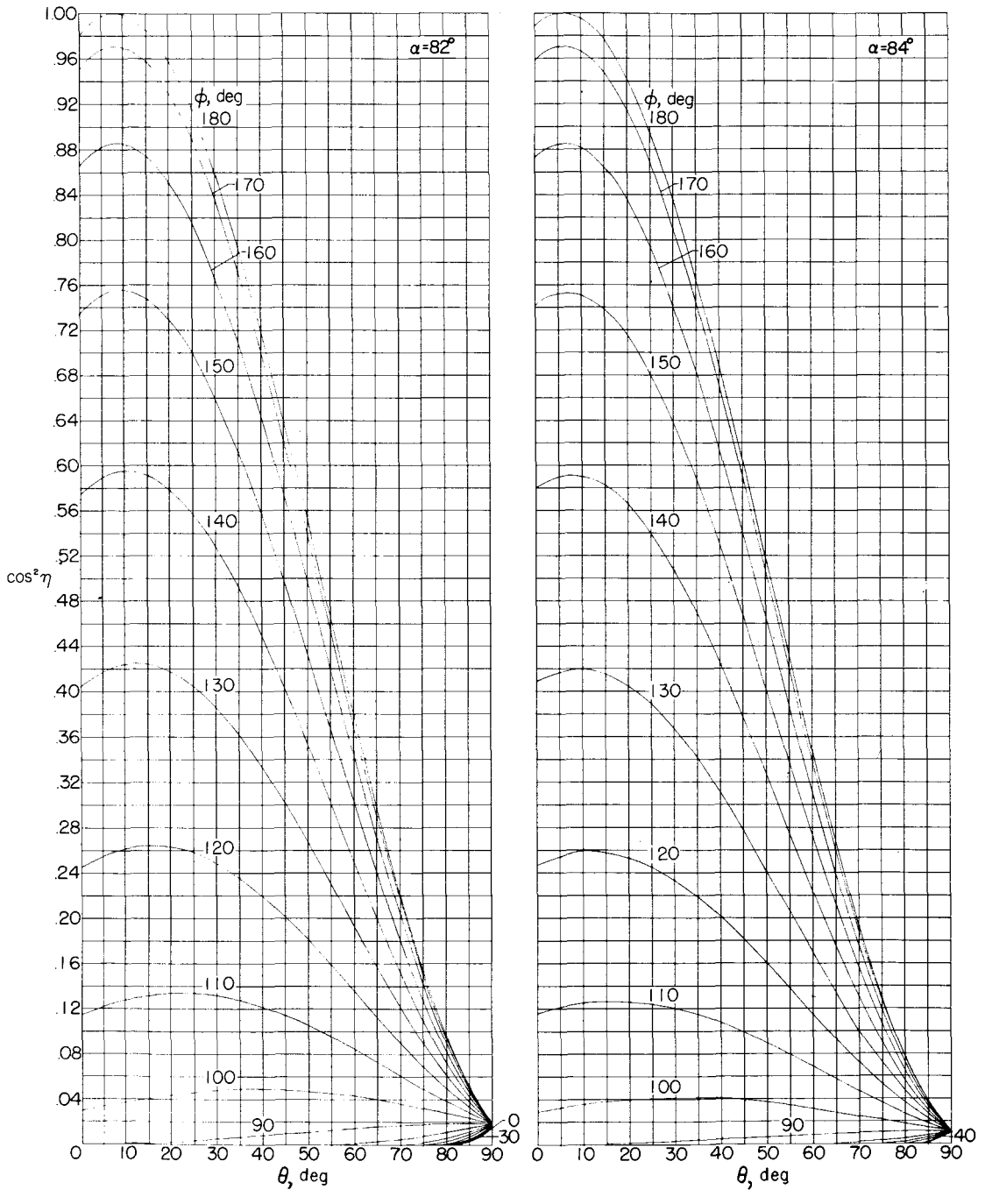

(j) $\alpha = 82^{\circ}$ and 84°.

Figure 5.- Continued.

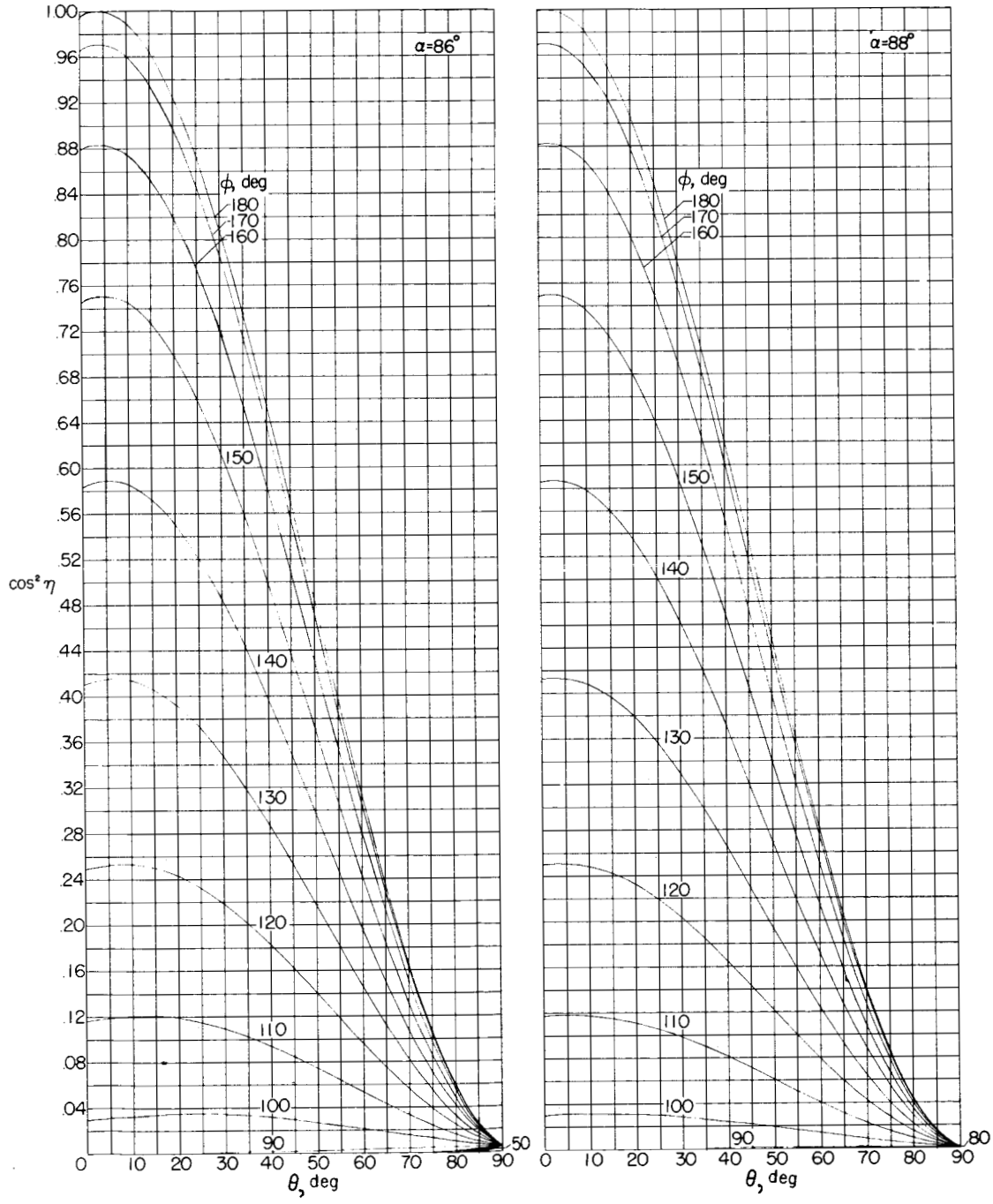

(k) $\alpha = 86^{\circ}$ and 88°.

Figure 5.- Continued.

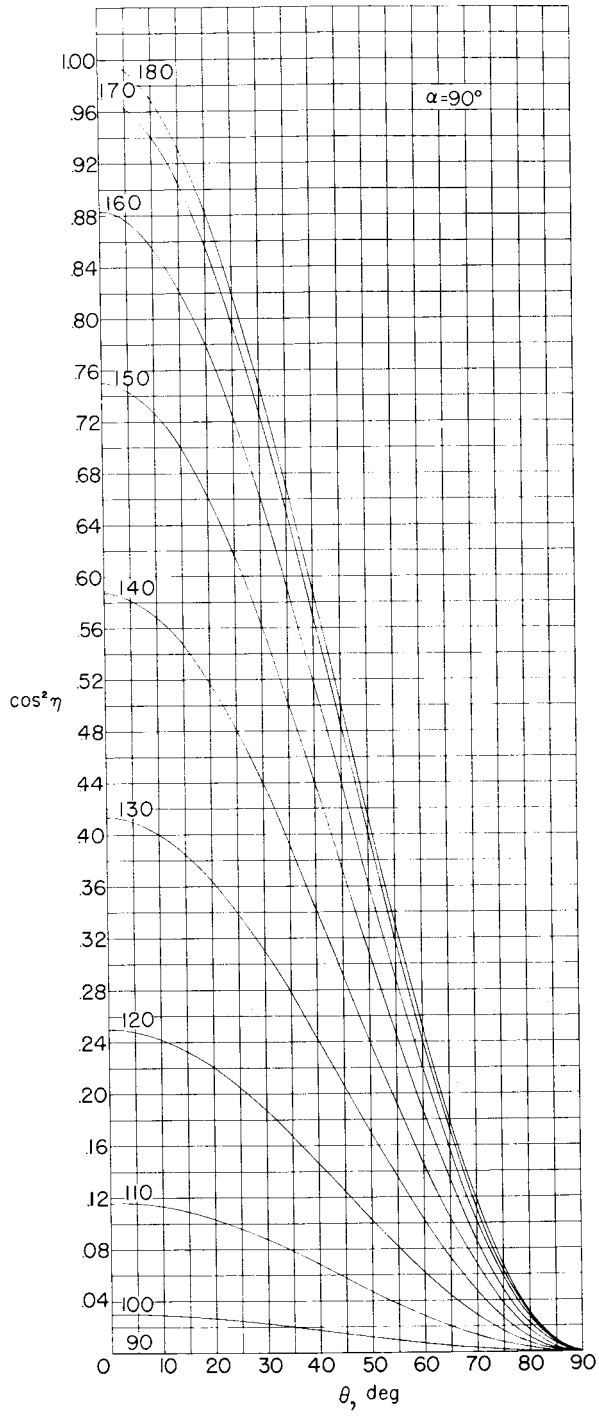

(l) $\alpha = 90^{\circ}$.

Figure 5.- Concluded.

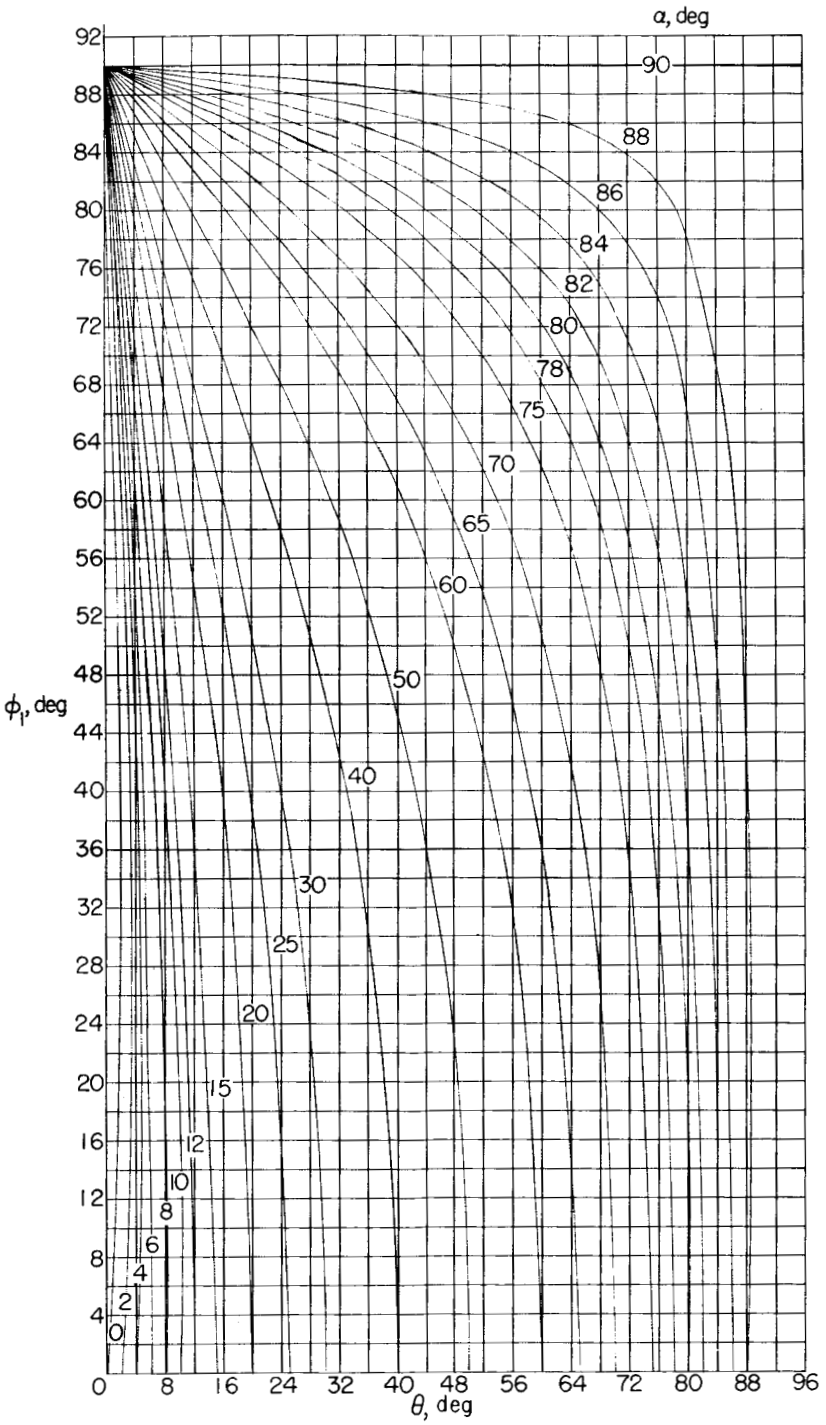

Figure 6.- Radial boundary, ϕ_1, of shadowed region of body of revolution.

L-516

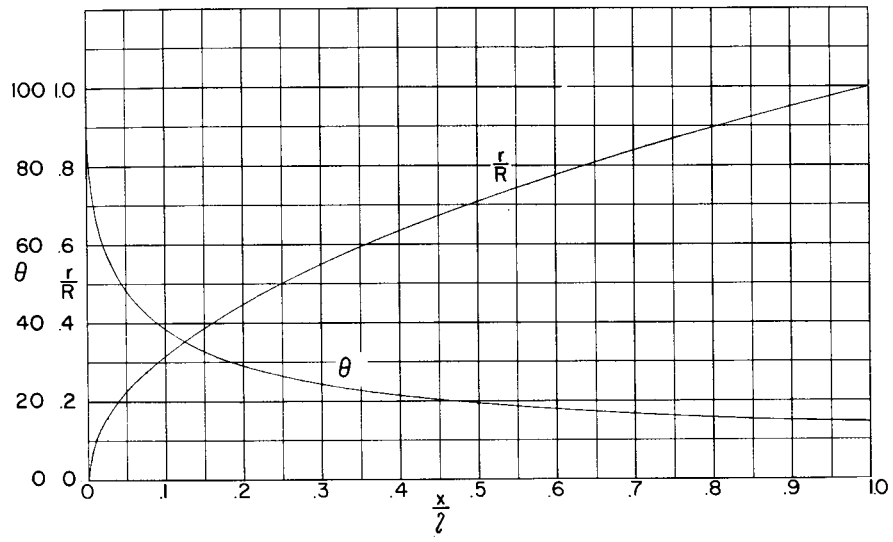

(a) Body ordinates, y/l, and surface slopes, θ.

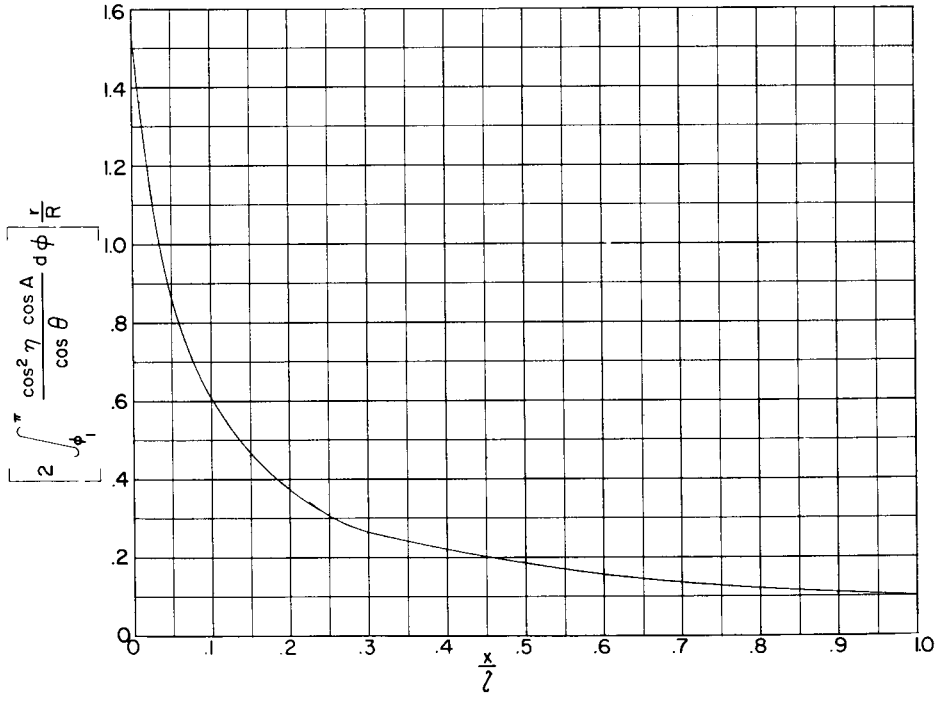

(b) Curve for axial-force-coefficient computation.

Figure 7.- Body of revolution and curves utilized in typical example at $\alpha = 6^{\circ}$.

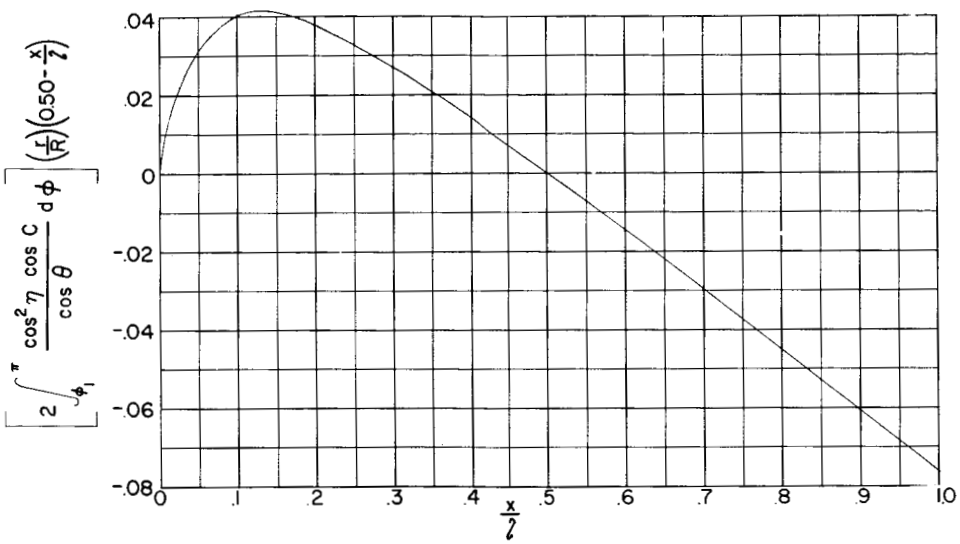

(c) Curve for pitching-moment-coefficient computation.

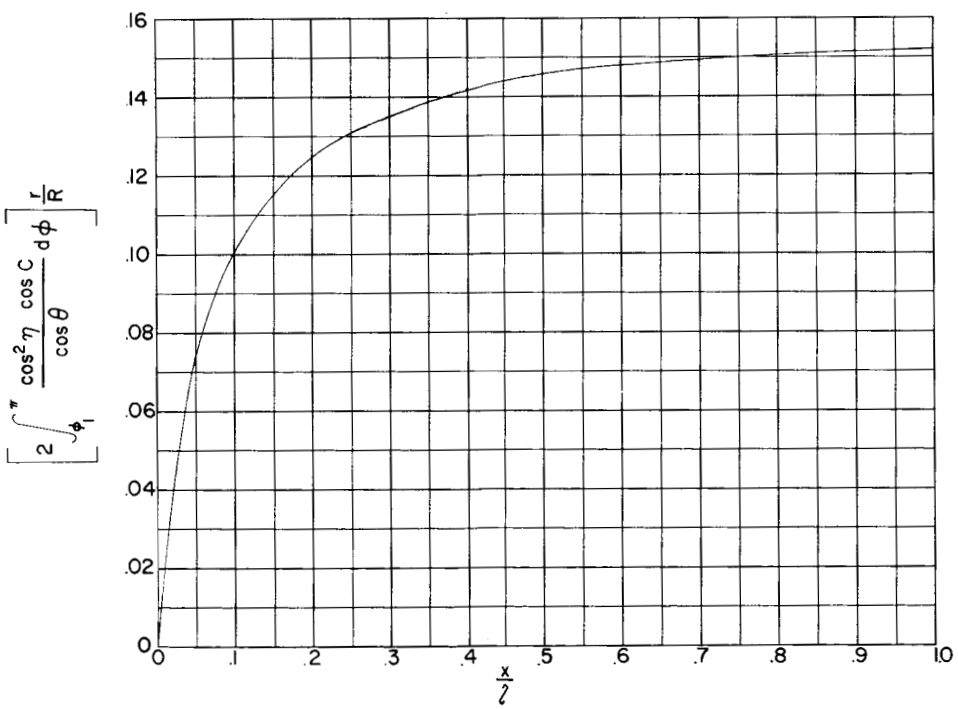

(d) Curve for normal-force-coefficient computation.

Figure 7.- Concluded.

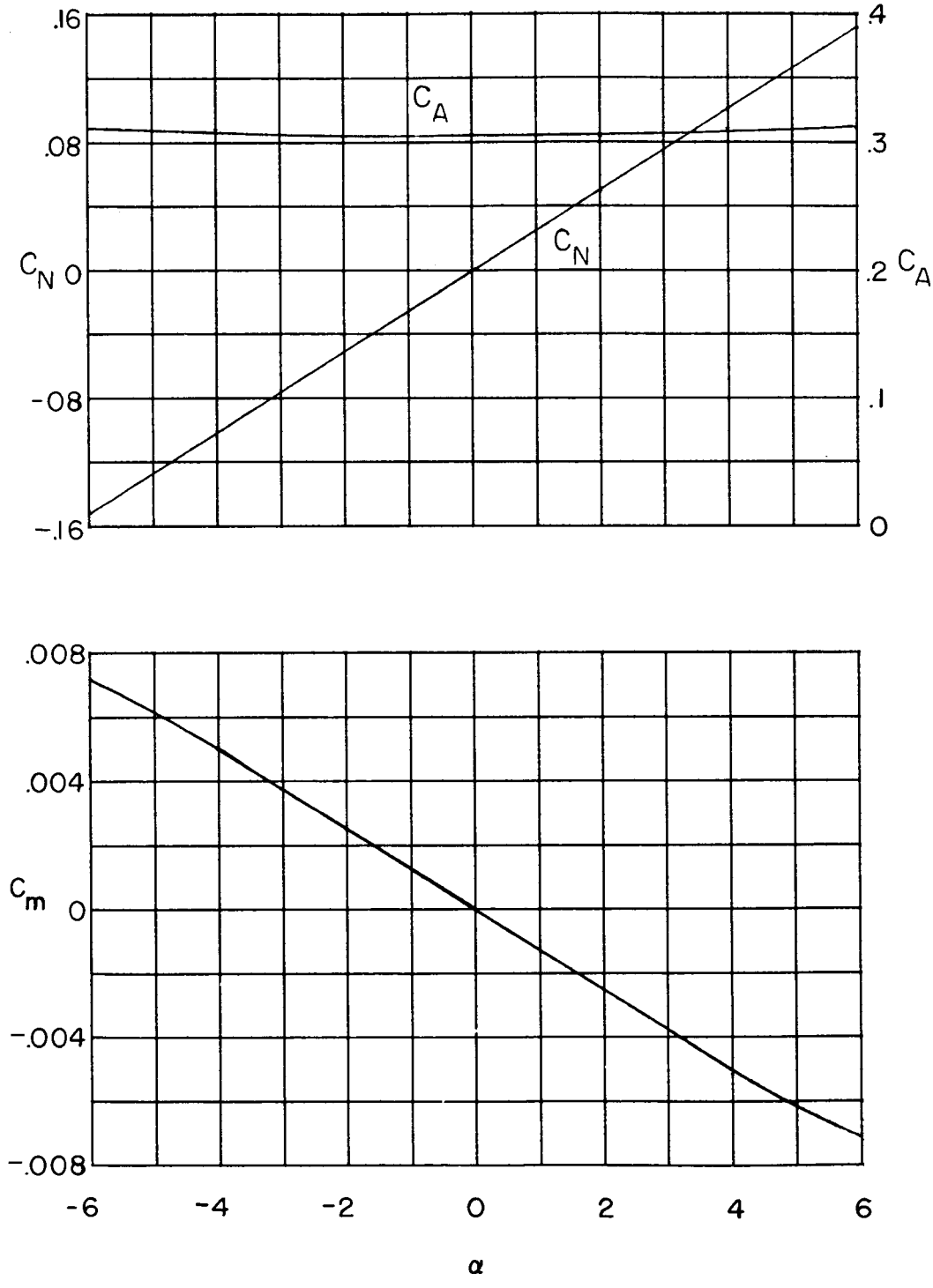

Figure 8.- Computed aerodynamic characteristics of fineness ratio 1, second-power body in air. M = 3.55.

L-516